NASA TECHNICAL REPORT

NASA TR R-155

NASA TR R-155

SPIN DYNAMICS OF MANNED SPACE STATIONS

by Peter R. Kurzhals and Claude R. Keckler

Langley Research Center
Langley Station, Hampton, Va.

NATIONAL AERONAUTICS AND SPACE ADMINISTRATION • WASHINGTON, D. C. • DECEMBER 1963

SPIN DYNAMICS OF MANNED SPACE STATIONS

By Peter R. Kurzhals and Claude R. Keckler

Langley Research Center
Langley Station, Hampton, Va.

NATIONAL AERONAUTICS AND SPACE ADMINISTRATION

For sale by the Office of Technical Services, Department of Commerce,
Washington, D.C. 20230 -- Price $1.50

SPIN DYNAMICS OF MANNED SPACE STATIONS*

By Peter R. Kurzhals and Claude R. Keckler

SUMMARY

An investigation of the spin dynamics of manned space stations has been conducted. The rigid-body equations of motion for arbitrary rotating stations were outlined and programed on an electronic data processing system. Docking impacts, attitude-system torques, mass unbalances, and transient crew motions were simulated in these equations, and a fourth-order Runge-Kutta integration procedure was used to determine the resultant station motion.

A toroidal configuration spinning about the axis of maximum moment of inertia was selected for the computer study, and results are presented in nondimensional form. The results are given as the traces of the station axis of symmetry in fixed space and as the time histories of the nondimensional angular velocities and attitudes of the station. This representation provides a simple physical picture of the station motion and of the time variation of the primary motion coordinates.

The results of this analysis indicated that the applied moments, mass unbalances, and crew motions produced undamped station wobbling, which to the crew would appear as a continuous rolling motion of the station floor. Since the undamped rolling motions produced by the disturbances, when coupled with the station rotation, could possibly lead to nausea and disorientation of the crew, a means of damping these motions is desirable. For this study two damping systems were considered, a gyroscopic wobble damper and a proportional jet damper. These systems, in general, were able to minimize the effects of the station wobble on the crew by reducing the apparent rolling motions to a small tilt of the station floor. The gyroscopic damping system was more efficient than the proportional jet system for small wobble angles, but the jet system was more effective than the gyroscopic system for the large wobble angles.

INTRODUCTION

Current concepts of manned space stations in general require rotation about a central axis to produce an artificial gravity field for the crew. Such rotation

*The information presented herein is based upon a thesis entitled "Spin Dynamics of Space Stations Under Transient and Steady-State Excitations and Stabilizing Responses" submitted by Peter R. Kurzhals in partial fulfillment of the requirements for the degree of Master of Science in Aerospace Engineering, Virginia Polytechnic Institute, Blacksburg, Virginia, June 1962.

also provides inherent stability and allows the station to maintain its orientation in space. However, there are dynamics problems arising from the wobbling motions of a spinning station under applied disturbances which must be investigated before any manned space stations can be safely operated.

In order to study the station dynamics it is necessary to define the equations of motion for a vehicle in space under the influence of various applied forcing parameters and to integrate these equations to determine the changes in the station's motion. A method of damping or minimizing such changes must then be provided.

Basic work on the dynamics of rotating bodies has been done in references 1 to 3, and equations of motion for an arbitrary spinning body are presented in reference 4. A number of simple computer solutions and approximate analytical results of these equations with steady-state conditions and specific configurations have also been obtained for the effects of rotating machinery, static mass disturbances, and applied moments.

The motion of a rotating cylinder with static product-of-inertia changes and external moments was considered by Grantham in reference 5, and a number of computer solutions were presented. This study was then extended, by approximate solutions developed by Leon in reference 6 and Suddath in reference 7, to take in several other configurations.

Subsequently, the use of a rotating precession wheel to damp the wobbling motions resulting from these applied excitations was investigated by Adams in reference 8 and by Suddath in reference 9. A method of damping by means of a jet system was also suggested by Martz in reference 10.

The present analysis extends the previous work to determine the transient and steady-state effects of a wide range of applied disturbances on the motion of rotating space stations with and without internal stability systems. The results of this study are of value in the design of any orbital rotating vehicle, since they can be used to predict the approximate dynamics of these vehicles and to define systems for minimizing any adverse wobbling motions.

SYMBOLS

a	acceleration of moving mass, ft/sec^2
G	damping moment, ft-lb
H	angular momentum, ft-lb-sec
I	moment or product of inertia, $slug\text{-}ft^2$
K_1, K_2	gain factors for gyroscopic wobble damper, sec
K_3, K_4	gain factors for jet damper, ft-lb-sec

L	total applied torque, ft-lb
M	external moment, ft-lb
m_s	mass of station without moving mass, slugs
m_m	moving mass, slugs
Q	constant defining center-of-gravity change, $\frac{m_m m_s}{m_s + m_m}$, slugs
r	radial coordinate of moving mass measured in $X_b Y_b$-plane, ft
T	nondimensional transfer time for moving mass, value of τ for mass transfer
t	time, sec
U	inclination angle between the Z_b- and the Z_{fs}-axis, deg (fig. 33)
V	angle between the X_b-axis and the $X_{fs}Y_{fs}$ reference plane, deg (fig. 33)
v	velocity of moving mass, ft/sec
W	angle between the Y_b-axis and the $X_{fs}Y_{fs}$ reference plane, deg (fig. 33)
X,Y,Z	reference axes
x,y,z	position coordinates of moving mass in body-axis system, ft
α	angular position, deg
γ	nondimensional inertia ratio, $I/I_{z,o}$
δ	position angle for Z_b-axis, deg
λ	nondimensional applied torque, $L/I_{z,o}\Omega_{z,o}^2$
ν	angular velocity of moving mass, radians/sec
τ	nondimensional time, $\Omega_{z,o}t$
ψ,θ,ϕ	modified Euler angles, deg (fig. 32)
Ω	body angular velocity, radians/sec
ω	nondimensional angular velocity, $\Omega/\Omega_{z,o}$

Subscripts:

av	average value
b	body coordinates
fs	fixed space coordinates
g	gyroscopic damper
lim	maximum or minimum value
t	total value
o	initial value
x,y,z	component for X-, Y-, or Z-axis
xy,xz,yz	component for the XY-, XZ-, or YZ-plane

A dot over a symbol denotes the derivative with respect to time.

A bar over a symbol denotes a vector.

A tilde (~) over a symbol denotes a matrix.

ANALYSIS

Presentation of Results

The nondimensionalized equations of motion developed in the appendix were programed on an electronic data processing system with a fourth-order Runge-Kutta integration procedure. The effects of various disturbances, with and without a flywheel and a proportional jet stability system, have been investigated for the configuration of figure 1 and the results are shown in figures 2 to 31.

The characteristic station motion for each type of disturbance is represented by the trace of the station axis of symmetry in fixed space. A solid line is used for this trace during the time the disturbance is applied, and a dashed line designates the trace after this time. The symmetry-axis trace is obtained by plotting the inclination angle U between the symmetry axis and a fixed reference line against the angular position δ of the symmetry axis measured in a plane perpendicular to the fixed reference line. This type of plot allows a simple visualization of the station motion with respect to a fixed coordinate system.

In addition, time histories of the attitudes and body angular velocities are presented for the example station. To allow a more general application of these results the time histories are given as nondimensional quantities,

independent of the station spin rate and size. This nondimensionalization process is described in the appendix.

The example station, shown in figure 1, has a diameter of 30 feet and would be capable of housing a crew of three astronauts. The basic station consists of a rigid central module and an inflatable outer torus connected to this module by four spokes. The central module, which contains most of the station instrumentation and equipment, would be used for the ascent and reentry phase of the mission while the erectable torus would serve as living quarters for the crew during the orbital flight.

For the present study the orbital weight of the example station is assumed as 8,100 pounds, the station moments of inertia are taken as

$$I_x = 7{,}500 \text{ slug-ft}^2$$

$$I_y = 7{,}500 \text{ slug-ft}^2$$

$$I_z = 10{,}000 \text{ slug-ft}^2$$

and the station is initially rotating about its Z-axis. The results obtained for this station should be indicative of the motions of any station spinning about its maximum axis of inertia. Wherever it is believed to be necessary, the effects of the station inertia distribution are also considered.

The stability-system parameters selected for the example station are

$$H_g = -\frac{1}{50} I_{z,o}\Omega_{z,o}$$

$$K_1 = 20 \text{ radians per radian/sec}$$

$$K_2 = 20 \text{ radians per radian/sec}$$

$$K_3 = -\frac{1}{20} I_{z,o}\Omega_{z,o}$$

$$K_4 = -\frac{1}{20} I_{z,o}\Omega_{z,o}$$

These system characteristics should represent reasonable values for space use. Thus, for the 30-foot station with a spin-axis moment of inertia of 10,000 slug-ft^2 and a spin rate of 0.5 radian/sec, the control-wheel angular momentum would be

$$H_g = -100 \text{ ft-lb-sec}$$

corresponding to a 25-pound steel disk rotating at 500 radians/sec. For the excitations investigated in this study, the jet system would need to develop a maximum moment about each axis of approximately 150 ft-lb. Such a moment could be produced by a jet mounted at the outside rim of the station and capable of about 10 pounds of thrust. The carbon dioxide waste within the station could conceivably be stored and used as a source of fuel for this system.

Applied Moments

The first disturbance to be considered is that corresponding to a docking torque or an attitude-jet thrust. This type of disturbance can be represented by a constant-moment pulse applied over a period of time. The basic response of the station and limiting wobble-angle values for this disturbance have been determined in reference 7, but a typical case will be presented here to illustrate the type of motion and the effectiveness of the damping systems.

A pulse moment given by

$$M_x = 125 \text{ ft-lb} \qquad (0 \leqq \tau \leqq 20)$$

$$M_x = 0 \qquad (\tau > 20)$$

was applied to the example station and the resultant undamped motion is shown in figure 2. The symmetry axis of the station can be seen to describe an epicycloidal path while the pulse moment is applied. After the moment is removed the station's angular-momentum vector remains constant. The symmetry axis then traces out a circle about the angular-momentum vector with a diameter defined by the angular velocities at cutoff.

The maximum wobble angle reached leads the initial applied moment vector by a right angle in fixed space and is given by

$$U_{lim} = 22^\circ$$

$$\delta = 90^\circ$$

The circle remaining after moment cutoff had a diameter of 6.5° with center at $U = 4.5^\circ$ and $\delta = 50^\circ$, corresponding to the position of the constant final angular-momentum vector. For all these motions the attitude angles and body rates oscillate continuously. The oscillation in the rates in turn produces a rolling of the centrifugal force or effective gravity vector. To a crew member in the station, this would appear as a continuous rolling motion of the station floor, much like the rolling motion of a moving ship.

Since it is desirable to minimize this motion, attempts at reducing the oscillations were made by using either the gyroscopic or the jet damping systems described in the appendix. The results for the applied moment, with these stability systems in operation, are presented in figures 3 and 4. The gyroscopic

damping shown in figure 3 reduces the maximum wobble angle, U_{lim}, from 22° to 19.5° during the application of the pulse moment. After removal of the moment, the station wobble is transformed into a steady spin about the axis corresponding to the station angular-momentum vector at cutoff. For the purpose of this study the wobble is assumed to be completely damped when the station motion is damped to within 1 percent of the final steady-state condition. The wobble after removal of the moment was damped in $\tau = 6.5$, which is approximately equal to one spin cycle ($\tau = 2\pi$) of the station.

For the jet stability system, as illustrated in figure 4, the maximum wobble angle is 18.1°, and the residual station wobble again damps to a steady spin about a new axis in space. However, this jet damping was less efficient timewise than the gyroscopic damping and approximately 10 spin cycles were required for the damping process.

The adverse effects of the docking torque or attitude-system moment on the crew of the station have been eliminated by both the stability systems. However, an attitude error remains and the station must correspondingly be provided with an attitude system capable of maintaining the station orientation in space, if this is required by the station mission.

Static Product-of-Inertia Disturbance

A second type of disturbance that may occur in a manned space station is that corresponding to a dynamic mass unbalance created by crew motions or cargo shifts. This disturbance can be approximately simulated by an instantaneous change in the products and moments of inertia of the station. The maximum disturbance for the example station would be one in which all three crew members moved simultaneously to an extreme position - that is, a position where they would produce a maximum dynamic unbalance - in the station. Assuming that each astronaut weighs 200 pounds, fully equipped, a mass unbalance of around 600 pounds would be created by this motion. From the geometry of the station the extreme position to which the crew, as represented by the equivalent 600-pound mass, could move is $x = 12$ feet, $y = 0$, and $z = 2.4$ feet in terms of the body-centered coordinate system. This motion would produce a product of inertia of $I_{xz} = 500$ slug-ft^2. The final moments of inertia after the mass transfer are approximately

$$I_x = 7{,}500 \text{ slug-ft}^2$$

$$I_y = 7{,}500 \text{ slug-ft}^2$$

$$I_z = 10{,}000 \text{ slug-ft}^2$$

and the station response for this disturbance is shown in figure 5.

The symmetry-axis trace is basically an epicycloid which results from rolling of the inertia ellipsoid on the fixed reference plane. In terms of Poinsot's construction of reference 2, this path is given by the polhode rolling on the

herpolhode in the reference plane. For the example, the herpolhode corresponds to the dashed circle in the figure and has its center in the initial product-of-inertia plane.

The maximum inclination angle thus lies in the plane of the applied product of inertia and is given by

$$U_{lim} = 21.8^{\circ}$$

$$\delta = 180^{\circ}$$

Physically, this can be interpreted in terms of the tendency of a body to spin about its maximum or minimum principal axis of inertia. When the spin axis is misalined with this axis, it will tend to move toward the principal axis. However, without damping, this movement will bring about an overshoot equal to the original misalinement, and the initial spin axis will then oscillate about the principal axis.

It is of interest to consider the effect of a variation in the moments of inertia on the wobble angles as produced by a mass disturbance in the station. Consequently a series of cases were run for a range of configurations, and limit magnitudes of the stability angles for various product-of-inertia disturbances were determined. These results are presented in figures 6 to 10 as nondimensional plots of the extreme values of the stability angles in terms of the inertia ratios I_x/I_z, I_y/I_z, and I_{xz}/I_z. Disturbance values of I_{xz}/I_z of 0.01, 0.02, 0.03, 0.04, and 0.05 are considered for I_y/I_z ratios of 0.1, 0.5, 1.0, 2.0, and 10.0 and a range of values of I_x/I_z. The resultant figures may be consulted for preliminary design work, and can be used to predict the approximate maximum wobbling motions for a given mass unbalance and inertia distribution.

The maximum inclination angle for the present case was derived as

$$U_{lim} = \tan^{-1} \frac{2I_{xz}}{I_z - I_x} \qquad \left(\frac{I_y}{I_z} \leqq 1\right)$$

and

$$U_{lim} = \frac{I_x}{I_z} \tan^{-1} \frac{2I_{xz}}{I_x - I_z} \qquad \left(\frac{I_y}{I_z} > 1\right)$$

and always occurred in the plane of the initial product of inertia. For configurations in which $I_y/I_z \leqq 1$, an increase in I_x/I_z produced an increase in U_{lim} and W_{lim}, while V_{lim} increased to its maximum at $I_x/I_z = 1$ and then decreased with any further increase in I_x. For configurations with $I_y/I_z > 1$ this trend was reversed, and an increase in I_x/I_z produced decreases in U_{lim}, V_{lim}, and W_{lim}.

These results agree with the statements of reference 1 in that the station wobble can be minimized by designing symmetrical configurations that spin about an axis corresponding to the maximum or minimum moment of inertia. Configurations that spin about an axis corresponding to an intermediate moment of inertia or one of two equal moments of inertia tend to be unstable.

To determine the effect of a damping system on these wobbling motions, the product-of-inertia disturbance, I_{xz} = 500 slug-ft^2, for the example station was applied with the jet or gyroscopic damper in operation. The corresponding station response is presented in figures 11 and 12. Figure 11 illustrates the station motion with the gyroscopic stability system. It can be seen that the symmetry-axis trace is damped to a circle. This damping was accomplished in approximately two spin cycles of the station. The jet stability system, which is shown in figure 12, produces a similar damping history and again results in a circular symmetry-axis trace. The damping time now is somewhat less than 10 spin cycles for the station.

Both damping systems reduced the maximum angle of attack for the undamped case and resulted in a circular motion of the symmetry axis. Since the body rates were constant for this circular motion the effects of the wobbling motions on the crew have been reduced to a small rotation of the centrifugal-force vector. To the crew this would appear as a tilt of the station floor.

Temporary Product-of-Inertia Disturbances

The effect of a temporary cargo shift or crew motion, in which a mass is moved so as to introduce products of inertia and then at some later time is returned to its original position, will now be discussed. A temporary product of inertia of

$$I_{xz} = 500 \text{ slug-ft}^2 \qquad (0 \leqq \tau \leqq 20)$$

$$I_{xz} = 0 \qquad (\tau > 20)$$

was applied to the example station. The result is shown in figure 13. The symmetry-axis trace follows an epicycloidal path until the mass disturbance is removed and then becomes a circle defined by the angular rates at the time of disturbance removal. The symmetry-axis trace and the time history for this case are quite similar to those for the applied moment.

It should be noted that the cusp of the epicycloidal motion corresponds to the condition of zero angular velocities in the plane of symmetry; thus,

$$\omega_x = \omega_y = 0$$

and the station is now spinning steadily about its original spin axis but with a different orientation in space. Since the residual circle and the resultant station wobble are defined by the angular velocities at the time of disturbance removal, it is at least theoretically possible to minimize the station wobble by

either removing the mass unbalance or introducing an equal and opposite unbalance simultaneously when the angular velocities ω_x and ω_y are both zero. This behavior may, of course, vary somewhat in an actual system since a true static product of inertia is not practically feasible.

The damped motion for the temporary product-of-inertia disturbance is presented in figures 14 and 15. With the gyroscopic stability system, as shown in figure 14, the station wobble is damped to a steady spin. Approximately one spin cycle was required for this damping after removal of the static product-of-inertia disturbance. With the jet system, which is illustrated in figure 15, damping to the pure spinning motion now takes place in about seven spin cycles.

Removal of the mass disturbance thus eliminates the circular symmetry-axis motion for the damped static product-of-inertia disturbance and results in a steady spin about the station axis of symmetry.

Combined Static Product-of-Inertia Disturbances

The motion of the station for a combined static product of inertia, or a mass shift to a general position in the station, was also studied to determine whether the additional terms in the equations of motion influence the basic station or stability-system response. Correspondingly, products of inertia given by

$$I_{xz} = 500 \text{ slug-ft}^2$$

$$I_{yz} = 500 \text{ slug-ft}^2$$

$$I_{xy} = 500 \text{ slug-ft}^2$$

were introduced for the example station, and the resulting motion is presented in figure 16. As expected, these results are similar to those for the single product-of-inertia disturbance. The station motion remains epicycloidal, and the maximum inclination angle again lies in the plane of the initial applied products of inertia. The stability angles and angular rates also oscillate about their principal-axis projections.

Damping for this excitation is shown in figures 17 and 18. The gyroscopic damping, illustrated in figure 17, reduces the station wobble to approximately half its initial amplitude in less than two spin cycles. However, a definite wobble, with amplitude equal to the angle between the initial Z_b-axis and the principal Z_b-axis, remains. With the proportional jet system more effective damping is obtained, as shown in figure 18. The station wobble now is reduced to a circular symmetry-axis trace about a new fixed space axis in about seven spin cycles.

A comparison of these two systems then shows that the gyroscopic damper with the full $\pm 90^\circ$ gimbal deflection used for this study is not capable of completely eliminating the wobble motions resulting from a general mass shift in the station.

The maximum gimbal angle in an actual system may thus have to be limited to some value lower than $\pm 90^{\circ}$ to avoid the possibility of residual wobbling motions. The jet damper, however, was able to reduce the station wobble to a steady conic motion with its characteristic circular symmetry-axis trace; hence the effects of the general mass transfer were restricted to a small rotation of the gravity vector.

Transient Radial Product-of-Inertia Disturbances

Since an instantaneously applied product of inertia does not represent the true effect of crew motion or cargo transfer in the station, a number of cases in which a transient mass shift is simulated will now be considered. Here, again, the maximum disturbance for the example station would be one in which all three astronauts moved simultaneously to the outside of the station in a radial direction, or around the rim of the station in a tangential direction. For the radial motion, corresponding to motion from the center to the rim of the station, it is assumed that the astronauts start at the position $x = 0$, $y = 0$, and $z = 0$, and move to the position $x = 12$ feet, $y = 0$, and $z = 2.4$ feet with a constant initial velocity and deceleration; thus, they arrive at their final position with zero velocity. The three nondimensional transfer times of 100, 20, and 4 corresponding to slow, average, and fast motion are considered, and the final moments of inertia after the mass transfer are

$$I_x = 7{,}500 \text{ slug-ft}^2$$

$$I_y = 7{,}500 \text{ slug-ft}^2$$

$$I_z = 10{,}000 \text{ slug-ft}^2$$

The final product of inertia after the mass transfer then becomes $I_{xz} = 500$ slug-ft^2, and thus these results can be directly compared with the results for the static case.

The station motion for the transient radial mass transfer is shown in figures 19 to 21. Figure 19 corresponds to a nondimensional transfer time T of 100; it can be seen that the epicycloidal trace of the symmetry axis has now degenerated into a spiral. After the mass has reached its final position the initial spin axis oscillates about the principal axis as shown by the dashed line. The inclination angle U reaches a maximum value of 14.5° and then oscillates about its principal-axis-of-inertia value with an amplitude of 6.5°. It should be noted that the spin moment of inertia is increased by the radial mass transfer, and the spin rate ω_z correspondingly decreases as the mass is moved outward. The wobble frequency, which is dependent on the spin rate, is also decreased. Figure 20 presents the station response for a nondimensional transfer time of 20. The symmetry-axis trace begins as a spiral and then becomes an epicycloid after the mass has reached its final position. The maximum value of the inclination angle U is 17.2°, and a wobble of 12.5° remains after the mass transfer. For

a further decrease in nondimensional transfer time to 4, as seen in figure 21, the symmetry-axis trace is trochoidal, the maximum inclination angle U has increased to 21.5°, and a residual oscillation of 21.5° is produced. All of these wobbling motions are less than those for the static product-of-inertia disturbance; thus the static inertia product can be considered a limiting case for the radial product-of-inertia disturbances.

The damping response of the station for a nondimensional transfer time of 20 is illustrated in figures 22 and 23. Figure 22 shows the resultant motion with the gyroscopic stability system. The station wobble is damped to a circular motion in which the symmetry axis describes a cone about its initial position in space. This coning motion occurs with a frequency equal to the spin frequency, and the stability angles and body rates are thus constant. Damping, after the radial mass transfer, takes place in about one spin cycle.

The station response with the jet system, presented in figure 23, is similar and leads to a coning motion with a small superimposed nutation. This damped motion is achieved in a little less than six spin cycles after completion of the radial mass transfer. As the body rates approach constant values with both stability systems, the effect of the transient radial mass transfer is again a small rotation of the gravity vector.

Transient Tangential Product-of-Inertia Disturbances

In general, crew motions in a spinning station will take place around the rim of the station to make maximum use of the artificial gravity field. Such tangential mass transfers will now be investigated. For the toroidal station and the extreme case of all three astronauts moving simultaneously, this tangential transfer may be simulated by moving the astronauts from the position $x = 12$ feet, $y = 0$, and $z = 2.4$ feet around the rim of the station at a constant velocity and in the direction of rotation, until they return to their original position. The nondimensional times required for this motion will again be taken as 100, 20, and 4. The moments of inertia after the mass transfer are

$$I_x = 7{,}500 \text{ slug-ft}^2$$

$$I_y = 7{,}500 \text{ slug-ft}^2$$

$$I_z = 10{,}000 \text{ slug-ft}^2$$

so that the initial and final product of inertia is $I_{xz} = 500$ slug-ft^2.

The response of the station is illustrated in figures 24 to 26. For the nondimensional transfer time T of 100, represented in figure 24, the result was a spiral symmetry-axis trace during the mass motion and, thereafter, a small wobble about the symmetry-axis position corresponding to the time the mass reached its final position. The inclination angle U increased to a maximum value of 164°, and 80° oscillations in V and W were produced. The spin rate ω_z

decreased and became negative, while the rates ω_y and ω_x exhibited large oscillations about zero.

The motion of the station for a transfer time of 20, as seen from figure 25, is similar and resulted in a maximum inclination angle of 152°. A further decrease in the transfer time to 4, shown in figure 26, reduced the spiral symmetry-axis trace to a trochoidal motion with wobble amplitudes only slightly larger than those for the static product-of-inertia case.

In general, response of the station to the transient tangential product-of-inertia disturbance was a precession of the initial spin axis with respect to the angular-momentum vector. The spinning motion of the station was transformed into a motion in which the initial spin axis described a cone about its original position in space. The magnitude of the resultant cone angle was largely dependent on the angular rate at which the mass moved and the corresponding rates of change of the products of inertia. For the example station, maximum cone angles five to seven times as large as those predicted for the static product-of-inertia case were reached for positive values of $\nu/\Omega_{z,o}$ given by

$$\frac{2\pi}{100} \leqq \frac{\nu}{\Omega_{z,o}} \leqq \frac{2\pi}{20}$$

Outside this range and for negative values of $\nu/\Omega_{z,o}$ the maximum wobble angles were approximately the same as those determined previously for the static product-of-inertia disturbance.

Since the excessive wobbling of the station caused by these disturbances cannot be tolerated by the crew, the efficiency of the stability system in reducing the station wobble is of great importance. The station motion with the stability system in operation is shown in figures 27 and 28. The gyroscopic stability system, presented in figure 27, produces slow damping of the residual symmetry-axis cone to a small principal-axis cone around the original symmetry-axis position. The damping is accomplished within 17 spin cycles after completion of the mass transfer.

For the proportional jet damping, illustrated in figure 28, the damping to the principal-axis cone is considerably more effective and occurs in about three spin cycles after the tangential motion. However, with the gyroscopic system the spin rate returns to approximately its initial value, whereas with the jet system the final spin rate is reduced to half this value. The wobble effects on the crew are again restricted to a small rotation of the gravity vector which produces an apparent tilt of the station floor.

General Transient Product-of-Inertia Disturbances

In addition to transient radial or tangential mass transfer it is, of course, possible to have combinations of mass transfer. One of these possible general transient motions is illustrated in figure 29. For this example the toroidal station was again used, and the three astronauts moved once around the rim at a

constant velocity from x = 12 feet, y = 0, z = -2.4 feet to x = 12 feet, y = 0, z = 2.4 feet with a nondimensional transfer time of 20. Motion occurs both along the rim and normal to the rim for this mass transfer. The final moments of inertia are assumed to be

$$I_x = 7{,}500 \text{ slug-ft}^2$$

$$I_y = 7{,}500 \text{ slug-ft}^2$$

$$I_z = 10{,}000 \text{ slug-ft}^2$$

The characteristic results were similar to those for the corresponding transient tangential case, although the maximum angle of attack only reached 125°. However, the residual cone traced out by the initial spin axis and the wobble frequency were greater than those for the pure tangential motion.

The stability-system response for the general product-of-inertia example was determined and is presented in figures 30 and 31. The gyroscopic damper, shown in figure 30, now reduces the residual symmetry-axis cone to the principal-axis cone about the initial spin-axis position in 22 spin cycles. The final spin rate of the station is increased slightly over its original value by this damping process.

The jet damping system, with the assumed control gains for the example station, produces an increase in the residual cone angle. This is caused by the magnitude of the damped wobble angle, which exceeds 90° after completion of the transient mass transfer. The stability system thus will damp toward an angle of 180°, resulting in a further magnification of the attitude error. From these results it appears that the station angular momentum, or the jet control gains, must be designed so as to limit the maximum station wobble to less than 90°.

Increasing the control gain factors to

$$K_3 = -\frac{1}{10} I_{z,o}\Omega_{z,o}$$

$$K_4 = -\frac{1}{10} I_{z,o}\Omega_{z,o}$$

changed this response to the damping illustrated in figure 31. Here the jet damper reduces the station wobble to the principal-axis cone in three spin cycles after the transient mass transfer. The final spin rate of the station again is approximately half its initial value, as was true for the pure tangential mass transfer.

The result of the general transient crew motions with the stability systems operating was, as expected, a small rotation of the gravity field. However, the extremely large wobble angles produced by these motions and the pure tangential

crew motions may make a small station, such as the one studied in this report, undesirable for an actual orbital mission.

CONCLUSIONS

A computer study of the dynamics of manned rotating space stations under static and transient excitations, without and with damping moments from either a gyroscopic or a jet stability system, indicates the following conclusions:

1. Docking moments and mass transfer disturbances resulted in undamped station wobbling, which to the crew would appear as a rolling motion of the station floor. This rolling motion, when coupled with the station rotation, could possibly lead to nausea and disorientation of the crew.

2. Transient mass transfer from the center of the station to the rim of the station or parallel to the spin axis of the station produced smaller wobble angles than those produced by static mass transfer where the mass was moved instantaneously.

3. Transient mass transfer around the rim of the station in the direction of rotation resulted in maximum wobble angles five to seven times as large as those for the static mass transfer. Motion in a direction opposite to the direction of rotation, however, did not produce any amplification of the static results.

4. A gyroscopic damping system was capable of transforming the station wobble produced by docking moments and temporary mass unbalances into a spin about the final angular-momentum vector of the station. Since some of these damped disturbances resulted in attitude errors, the station must be provided with an additional system capable of maintaining the station orientation in space, if such orientation is required by the station mission. For a continuously applied dynamic mass unbalance, the gyroscopic system reduced the resultant wobbling motion to a smaller wobble or a spin about the maximum principal axis of inertia.

5. A proportional jet damping system reduced the station wobble for all disturbances to a steady spinning motion about an axis defined by the principal inertia axes of the station. For temporary disturbances the spin vector for this motion coincided with the station symmetry axis, while for continuously applied disturbances this vector was alined with the principal axis of inertia. The effects of the continuously applied disturbances and the resultant wobble were thus reduced to a rotation of the gravity vector or a small apparent tilt of the station floor.

6. The gyroscopic damping system produced faster damping than the proportional jet system for small wobble angles, but the jet system produced faster damping than the gyroscopic system at the larger wobble angles.

Langley Research Center,
National Aeronautics and Space Administration,
Langley Station, Hampton, Va., October 17, 1962.

APPENDIX

EQUATIONS OF MOTION

Derivation of Equations of Motion

The motion of the space station will be defined with reference to a moving body-axis system, and the body axes will then be related to space-fixed axes by means of a set of modified Euler angles. These modified Euler angles, which are illustrated in figure 32, result from three consecutive rotations. The first rotation, about the Z_{fs}-axis, carries the X_{fs}- and the Y_{fs}-axis through an angle ψ measured in a horizontal plane. The second rotation, about the new Y_{fs}-axis, then takes the X_{fs}- and Z_{fs}-axis through an angle θ measured in a vertical plane. Finally, the third rotation, about the new X_{fs}-axis, carries the Y_{fs}- and the Z_{fs}-axis through an angle ϕ, measured in an inclined plane, to give the X_b-, Y_b-, and Z_b-axis.

The modified Euler angles may be described mathematically by expressing the angular rates about the body axes in terms of the rotations $\dot{\psi}$, $\dot{\theta}$, and $\dot{\phi}$. These angular rates then become

$$\left.\begin{aligned} \Omega_x &= \dot{\phi} - \dot{\psi} \sin \theta \\ \Omega_y &= \dot{\theta} \cos \phi + \dot{\psi} \sin \phi \cos \theta \\ \Omega_z &= \dot{\psi} \cos \phi \cos \theta - \dot{\theta} \sin \phi \end{aligned}\right\} \tag{1}$$

and solving for the rotations results in

$$\left.\begin{aligned} \dot{\phi} &= \Omega_x + \Omega_y \tan \theta \sin \phi + \Omega_z \tan \theta \cos \phi \\ \dot{\theta} &= \Omega_y \cos \phi - \Omega_z \sin \phi \\ \dot{\psi} &= \Omega_z \cos \phi \sec \theta + \Omega_y \sin \phi \sec \theta \end{aligned}\right\} \tag{2}$$

Integration of these differential equations yields the Euler angles for the system.

To aid in visualizing the station motion, an additional set of stability angles will be introduced. The angles are shown in figure 33, and are given by

$$\left.\begin{aligned} U &= \cos^{-1}(\cos \phi \cos \theta) \\ V &= -\theta \\ W &= \sin^{-1}(\sin \phi \cos \theta) \end{aligned}\right\} \tag{3}$$

Physically, U is the inclination angle between the Z_b- and the Z_{fs}-axis, and V and W are the angles the X_b- and the Y_b-axis make with the $X_{fs}Y_{fs}$ reference plane. The stability angles provide a simple means of determining the deviation of the body axes from a fixed reference plane and position, and can be used as check data for a stability or attitude-control system.

The trace of the station Z-axis in fixed space can be obtained by preparing a polar plot with the stability angle U as the radial coordinate and an angle δ as the angular coordinate. The angle δ is calculated from the previously computed Euler angles by means of the formula

$$\delta = \psi - \tan^{-1}\left(\frac{\tan \phi}{\sin \theta}\right) \tag{4}$$

In order to determine the stability and modified Euler angles, however, the angular velocities about the body axes must first be found. These velocities can be calculated from the expression for the time rate of change of angular momentum which states that

$$\dot{\bar{H}}_{fs} = \bar{L}_{fs} \tag{5}$$

or, with respect to body coordinates,

$$\dot{\bar{H}}_b + \bar{\Omega}_b \times \bar{H}_b = \bar{L}_b \tag{6}$$

Expanding equation (6) into the component expressions for the body axes yields

$$\left.\begin{aligned} \dot{H}_x - \Omega_z H_y + \Omega_y H_z &= L_x \\ \dot{H}_y - \Omega_x H_z + \Omega_z H_x &= L_y \\ \dot{H}_z - \Omega_y H_x + \Omega_x H_y &= L_z \end{aligned}\right\} \tag{7}$$

The angular momentum is defined by the linear matrix equation

$$\tilde{H} = \tilde{I}\tilde{\Omega} \tag{8}$$

so that

$$\left.\begin{aligned} H_x &= I_x\Omega_x - I_{xy}\Omega_y - I_{xz}\Omega_z \\ H_y &= I_y\Omega_y - I_{yx}\Omega_x - I_{yz}\Omega_z \\ H_z &= I_z\Omega_z - I_{zy}\Omega_y - I_{zx}\Omega_x \end{aligned}\right\} \tag{9}$$

and substituting for the angular-momentum terms of equations (7), using equations (9), results in the final equations of motion:

$$
\left.
\begin{aligned}
L_x &= I_x\dot{\Omega}_x - I_{xy}\dot{\Omega}_y - I_{xz}\dot{\Omega}_z + \dot{I}_x\Omega_x - \dot{I}_{xy}\Omega_y - \dot{I}_{xz}\Omega_z \\
&\quad - \Omega_z\left(I_y\Omega_y - I_{yz}\Omega_z - I_{yx}\Omega_x\right) + \Omega_y\left(I_z\Omega_z - I_{zx}\Omega_x - I_{zy}\Omega_y\right) \\
L_y &= I_y\dot{\Omega}_y - I_{yz}\dot{\Omega}_z - I_{yx}\dot{\Omega}_x + \dot{I}_y\Omega_y - \dot{I}_{yz}\Omega_z - \dot{I}_{yx}\Omega_x \\
&\quad - \Omega_x\left(I_z\Omega_z - I_{zx}\Omega_x - I_{zy}\Omega_y\right) + \Omega_z\left(I_x\Omega_x - I_{xy}\Omega_y - I_{xz}\Omega_z\right) \\
L_z &= I_z\dot{\Omega}_z - I_{zx}\dot{\Omega}_x - I_{zy}\dot{\Omega}_y + \dot{I}_z\Omega_z - \dot{I}_{zx}\Omega_x - \dot{I}_{zy}\Omega_y \\
&\quad - \Omega_y\left(I_x\Omega_x - I_{xy}\Omega_y - I_{xz}\Omega_z\right) + \Omega_x\left(I_y\Omega_y - I_{yz}\Omega_z - I_{yx}\Omega_x\right)
\end{aligned}
\right\} \tag{10}
$$

A simultaneous solution of equations (10) for the body rates, and of equations (2) for the Euler angles, then completely defines the angular motion of the space station.

Nondimensional Equations of Motion

To increase the range of application of the results of this investigation, the equations of motion are nondimensionalized by introducing a nondimensional time τ and an inertia matrix $\tilde{\gamma}$ defined by

$$
\tau = \Omega_{z,o}t \qquad\qquad \tilde{\gamma} = \frac{\tilde{I}}{I_{z,o}} \tag{11}
$$

The nondimensional angular-velocity vector then becomes

$$
\bar{\omega} = \frac{d\alpha}{d\tau} = \frac{d\alpha}{dt}\frac{dt}{d\tau} = \frac{\bar{\Omega}}{\Omega_{z,o}} \tag{12}
$$

and the higher order derivatives, in a similar fashion, are derived as

$$
\left.
\begin{aligned}
\dot{\bar{\omega}} &= \frac{d\bar{\omega}}{d\tau} = \frac{\dot{\bar{\Omega}}}{\Omega_{z,o}^2} \\
\dot{\tilde{\gamma}} &= \frac{d\gamma}{d\tau} = \frac{\dot{\tilde{I}}}{I_{z,o}\Omega_{z,o}}
\end{aligned}
\right\} \tag{13}
$$

The equations of motion in terms of these nondimensional parameters are, from equations (10),

$$\left.\begin{aligned}
\lambda_x &= \gamma_x\dot{\omega}_x - \gamma_{xy}\dot{\omega}_y - \gamma_{xz}\dot{\omega}_z + \dot{\gamma}_x\omega_x - \dot{\gamma}_{xy}\omega_y - \dot{\gamma}_{xz}\omega_z \\
&\quad - \omega_z\left(\gamma_y\omega_y - \gamma_{yz}\omega_z - \gamma_{yx}\omega_x\right) + \omega_y\left(\gamma_z\omega_z - \gamma_{zx}\omega_x - \gamma_{zy}\omega_y\right) \\
\lambda_y &= \gamma_y\dot{\omega}_y - \gamma_{yz}\dot{\omega}_z - \gamma_{yx}\dot{\omega}_x + \dot{\gamma}_y\omega_y - \dot{\gamma}_{yz}\omega_z - \dot{\gamma}_{yx}\omega_x \\
&\quad - \omega_x\left(\gamma_z\omega_z - \gamma_{zx}\omega_x - \gamma_{zy}\omega_y\right) + \omega_z\left(\gamma_x\omega_x - \gamma_{xy}\omega_y - \gamma_{xz}\omega_z\right) \\
\lambda_z &= \gamma_z\dot{\omega}_z - \gamma_{zx}\dot{\omega}_x - \gamma_{zy}\dot{\omega}_y + \dot{\gamma}_z\omega_z - \dot{\gamma}_{zx}\omega_x - \dot{\gamma}_{zy}\omega_y \\
&\quad - \omega_y\left(\gamma_x\omega_x - \gamma_{xy}\omega_y - \gamma_{xz}\omega_z\right) + \omega_x\left(\gamma_y\omega_y - \gamma_{yz}\omega_z - \gamma_{yx}\omega_x\right)
\end{aligned}\right\} \qquad (14)$$

where

$$\bar{\lambda} = \frac{\bar{L}}{I_{z,o}\Omega_{z,o}^2} \qquad (15)$$

The nondimensional Euler angle rates can now be expressed from equations (2) as

$$\left.\begin{aligned}
\frac{d\phi}{d\tau} &= \omega_x + \omega_y \tan\theta \sin\phi + \omega_z \tan\theta \cos\phi \\
\frac{d\theta}{d\tau} &= \omega_y \cos\phi - \omega_z \sin\phi \\
\frac{d\psi}{d\tau} &= \omega_z \cos\phi \sec\theta + \omega_y \sin\phi \sec\theta
\end{aligned}\right\} \qquad (16)$$

and again

$$\frac{d\phi}{d\tau} = \frac{\dot{\phi}}{\Omega_{z,o}} \qquad \frac{d\theta}{d\tau} = \frac{\dot{\theta}}{\Omega_{z,o}} \qquad \frac{d\psi}{d\tau} = \frac{\dot{\psi}}{\Omega_{z,o}} \qquad (17)$$

It may be seen from these equations that the form of the Euler and stability angles is not affected by the nondimensionalization process.

Disturbance Parameters and Stability Torques

Before equations (14) can be solved, the moments and products of inertia, and the applied torques acting on the station, must be defined. The inertia terms will, of course, be dependent upon any mass transfer within the station and must be written to include the effects of crew movements and cargo shifts. If the moving mass is simulated by an equivalent mass m_m, the moments and products of

inertia can be written as functions of their initial values and of the position coordinates of the equivalent mass as follows:

$$\left.\begin{aligned} I_x &= I_{x,o} + Q(y^2 + z^2) \\ I_y &= I_{y,o} + Q(x^2 + z^2) \\ I_z &= I_{z,o} + Q(x^2 + y^2) \\ I_{xy} &= Q(xy) \\ I_{xz} &= Q(xz) \\ I_{yz} &= Q(yz) \end{aligned}\right\} \tag{18}$$

where the mass parameter Q is given by

$$Q = \frac{m_m m_s}{m_s + m_m} \tag{19}$$

The time rates of change of the inertia expressions in equations (10) then are

$$\left.\begin{aligned} \dot{I}_x &= 2Q(y\dot{y} + z\dot{z}) \\ \dot{I}_y &= 2Q(x\dot{x} + z\dot{z}) \\ \dot{I}_z &= 2Q(x\dot{x} + y\dot{y}) \\ \dot{I}_{xy} &= Q(x\dot{y} + y\dot{x}) \\ \dot{I}_{xz} &= Q(x\dot{z} + z\dot{x}) \\ \dot{I}_{yz} &= Q(y\dot{z} + z\dot{y}) \end{aligned}\right\} \tag{20}$$

For the present investigation the position coordinates x, y, and z are expressed as

$$\left.\begin{aligned} x &= \tfrac{1}{2} a_{x,o} t^2 + v_{x,o} t + x_o + r \cos \nu t \\ y &= \tfrac{1}{2} a_{y,o} t^2 + v_{y,o} t + y_o + r \sin \nu t \\ z &= \tfrac{1}{2} a_{z,o} t^2 + v_{z,o} t + z_o \end{aligned}\right\} \tag{21}$$

and their time derivatives become

$$\left.\begin{aligned} \dot{x} &= a_{x,o}t + v_{x,o} - r\nu \sin \nu t \\ \dot{y} &= a_{y,o}t + v_{y,o} + r\nu \cos \nu t \\ \dot{z} &= a_{z,o}t + v_{z,o} \end{aligned}\right\} \tag{22}$$

The mass-transfer coordinates described in equations (21) and (22) are based partly on the assumption that the station is initially spinning about the Z_b-axis. This assumption will be adhered to throughout the analysis. Two basic types of motion are then defined by these equations. The first type is motion with constant initial acceleration and constant initial velocity, starting from some initial position; the second type is mass transfer in the plane of rotation, along a circular path and with constant angular velocity. These motions should approximately simulate crew movements and cargo shifts within a rotating space station.

In addition to the mass-transfer disturbances, the rotating space station will in general be subjected to applied torques such as external and stability moments. The applied torques can be written as

$$\overline{L} = \overline{M} + \overline{G} \tag{23}$$

where the external moments $\overline{M}$ represent attitude-jet thrusts or docking impacts, and the stability moments $\overline{G}$ represent the stabilizing moments of a wobble-damping system.

The external moments acting on the station are given by

$$M_x = M_{x,o} \qquad M_y = M_{y,o} \qquad M_z = M_{z,o} \tag{24}$$

and describe the constant moments of a pulse-jet system or a docking impact.

The stability moments, on the other hand, are directly dependent on the type of damping system used. Here two systems will be considered, a primary and a backup system. The basic system is a gyroscopic wobble damper such as that shown in figure 34 and discussed in reference 8. This system consists of a flywheel mounted on double gimbals, rotating at a constant rate with its spin vector parallel to the station spin axis. When a disturbance is introduced, the spin axis of the flywheel is reoriented by a programed change in the gimbal attitude to create a precessional torque which opposes the applied disturbance. The gimbal axes will be initially oriented along the X and Y station axes as shown in figure 35. The gimbal angles are then controlled by an analog programer so that

$$\alpha_{x,g} = K_1\Omega_x \qquad \alpha_{y,g} = K_2\Omega_y \tag{25}$$

with a stop at the optimum gimbal deflection of $\pm 90^\circ$. The total angular velocity of the flywheel axis with respect to the station axes is

$$\left.\begin{aligned} \Omega_{x,t} &= \Omega_x + \dot{\alpha}_{x,g} \\ \Omega_{y,t} &= \Omega_y + \dot{\alpha}_{y,g} \cos \alpha_{x,g} \\ \Omega_{z,t} &= \Omega_z + \dot{\alpha}_{y,g} \sin \alpha_{x,g} \end{aligned}\right\} \tag{26}$$

The gyroscopic moments, in terms of the flywheel angular momentum H_g and these total angular rates, then become

$$\left.\begin{aligned} G_x &= \Omega_{y,t} H_{z,g} - \Omega_{z,t} H_{y,g} \\ G_y &= \Omega_{z,t} H_{x,g} - \Omega_{x,t} H_{z,g} \\ G_z &= \Omega_{x,t} H_{y,g} - \Omega_{y,t} H_{x,g} \end{aligned}\right\} \tag{27}$$

where, from figure 35,

$$\left.\begin{aligned} H_{x,g} &= H_g \sin \alpha_{y,g} \\ H_{y,g} &= -H_g \cos \alpha_{y,g} \sin \alpha_{x,g} \\ H_{z,g} &= H_g \cos \alpha_{y,g} \cos \alpha_{x,g} \end{aligned}\right\} \tag{28}$$

Substituting in equations (27) from equations (25), (26), and (28) yields the final expressions for the gyroscopic moments:

$$\left.\begin{aligned} G_x &= \left(H_g \cos K_2\Omega_y \cos K_1\Omega_x\right)\left(\Omega_y + K_2\dot{\Omega}_y \cos K_1\Omega_x\right) \\ &\quad + \left(H_g \cos K_2\Omega_y \sin K_1\Omega_x\right)\left(\Omega_z + K_2\dot{\Omega}_y \sin K_1\Omega_x\right) \\ G_y &= \left(H_g \sin K_2\Omega_y\right)\left(\Omega_z + K_2\dot{\Omega}_y \sin K_1\Omega_x\right) \\ &\quad - \left(H_g \cos K_2\Omega_y \cos K_1\Omega_x\right)\left(\Omega_x + K_1\dot{\Omega}_x\right) \\ G_z &= -\left(H_g \cos K_2\Omega_y \sin K_1\Omega_x\right)\left(\Omega_x + K_1\dot{\Omega}_x\right) \\ &\quad - \left(H_g \sin K_2\Omega_y\right)\left(\Omega_y + K_2\dot{\Omega}_y \cos K_1\Omega_x\right) \end{aligned}\right\} \tag{29}$$

The linear gain factors used in equations (29) imply the assumption of a perfect servomechanism in the programing unit; on the basis of the frequencies involved, this assumption should introduce very little error.

It is generally desirable to have a backup system in case of malfunction or failure of the primary damper. In this study the secondary system will utilize variable-moment jets which provide a moment proportional to the magnitude of the excitation. Such a system could be achieved in practice by regulating the mass flow through jets alined normal to the station X- and Y-axis as shown in figure 36. The system would use the output of two rate gyros measuring rates about these axes, and after modifying this output to define a rate error from a mean rate value, would actuate appropriate control valves to provide the damping moments required to reduce the station wobble to a steady spinning or cone-type motion. The mean rate value could be determined by periodic integration of the rate signal over a time increment greater than the spin period of the station.

The magnitudes of the moments exerted on the station by this system can then be represented by

$$G_x = K_3\left(\Omega_x - \Omega_{x,av}\right) \qquad G_y = K_4\left(\Omega_y - \Omega_{y,av}\right) \tag{30}$$

where the average angular velocities are taken as the projection of the total angular velocity vector on the station principal axes of inertia.

REFERENCES

1. MacMillan, William Duncan: Theoretical Mechanics. Dynamics of Rigid Bodies. Dover Pub., Inc., c.1936.

2. Routh, Edward John: Dynamics of a System of Rigid Bodies (Advanced Part). Sixth ed., Dover Pub., Inc., 1905.

3. Goldstein, Herbert: Classical Mechanics. Addison-Wesley Pub. Co., Inc. (Reading, Mass.), c.1959.

4. Anon.: Fundamentals of Design of Piloted Aircraft Flight Control Systems. Vol. II - Dynamics of the Airframe. Rep. AE-61-4, Bur. Aero., Feb. 1953.

5. Grantham, William D.: Effects of Mass-Loading Variations and Applied Moments on Motion and Control of a Manned Rotating Space Vehicle. NASA TN D-803, 1961.

6. Leon, H. I.: Spin Dynamics of Rockets and Space Vehicles in Vacuum. TR-59-0000-00787, Space Tech. Labs., Inc., Sept. 16, 1959.

7. Suddath, Jerrold H.: A Theoretical Study of the Angular Motions of Spinning Bodies in Space. NASA TR R-83, 1961.

8. Adams, J. J.: Study of an Active Control System for a Spinning Body. NASA TN D-905, 1961.

9. Suddath, Jerrold H.: Use of an Inertia Sphere to Damp the Angular Motions of Spinning Space Vehicles. NASA TR R-137, 1962.

10. Martz, C. William: Method for Approximating the Vacuum Motions of Spinning Symmetrical Bodies With Nonconstant Spin Rates. NASA TR R-115, 1961.

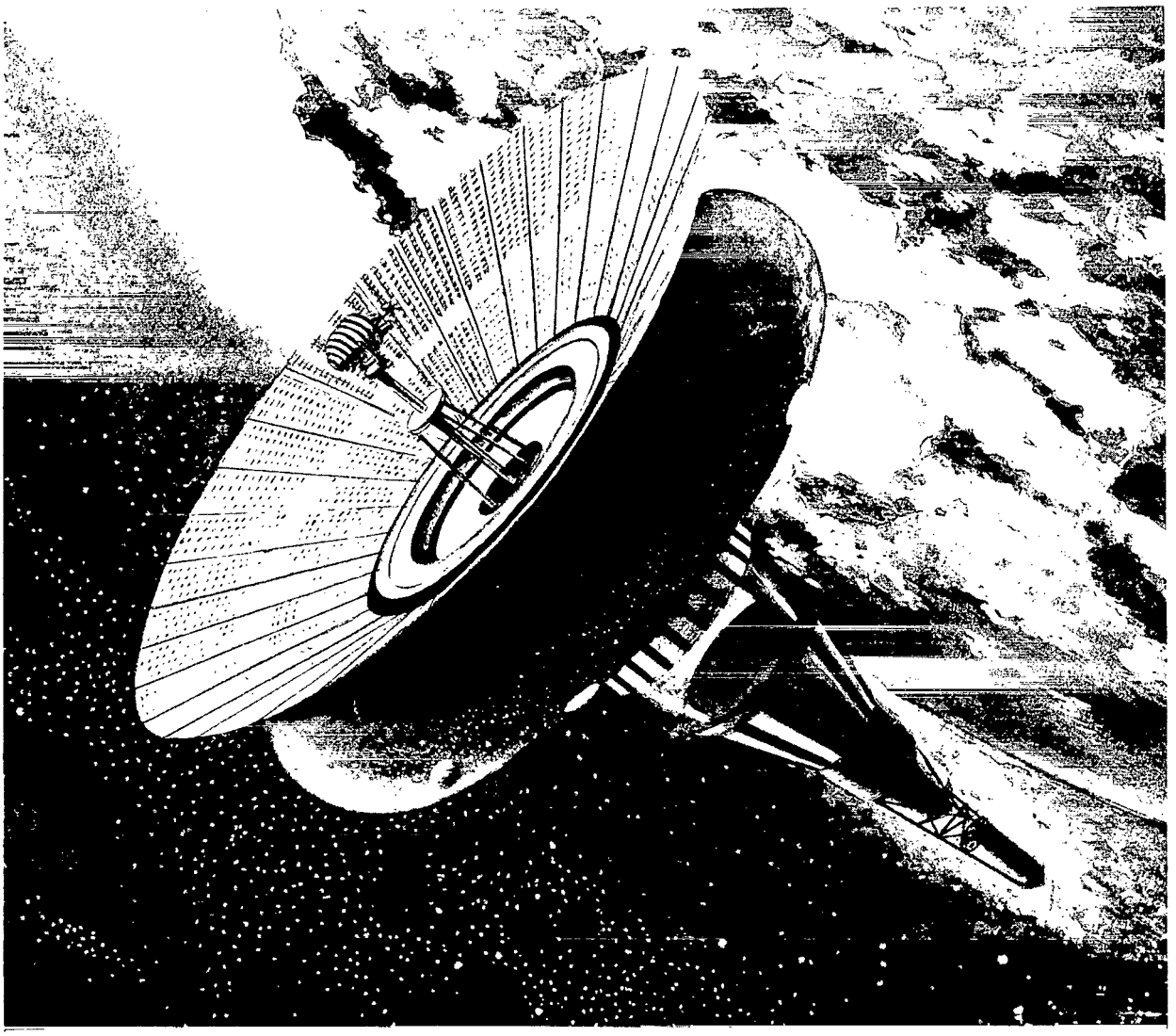

Figure 1.- Sketch of representative space-station configuration. L-60-7389

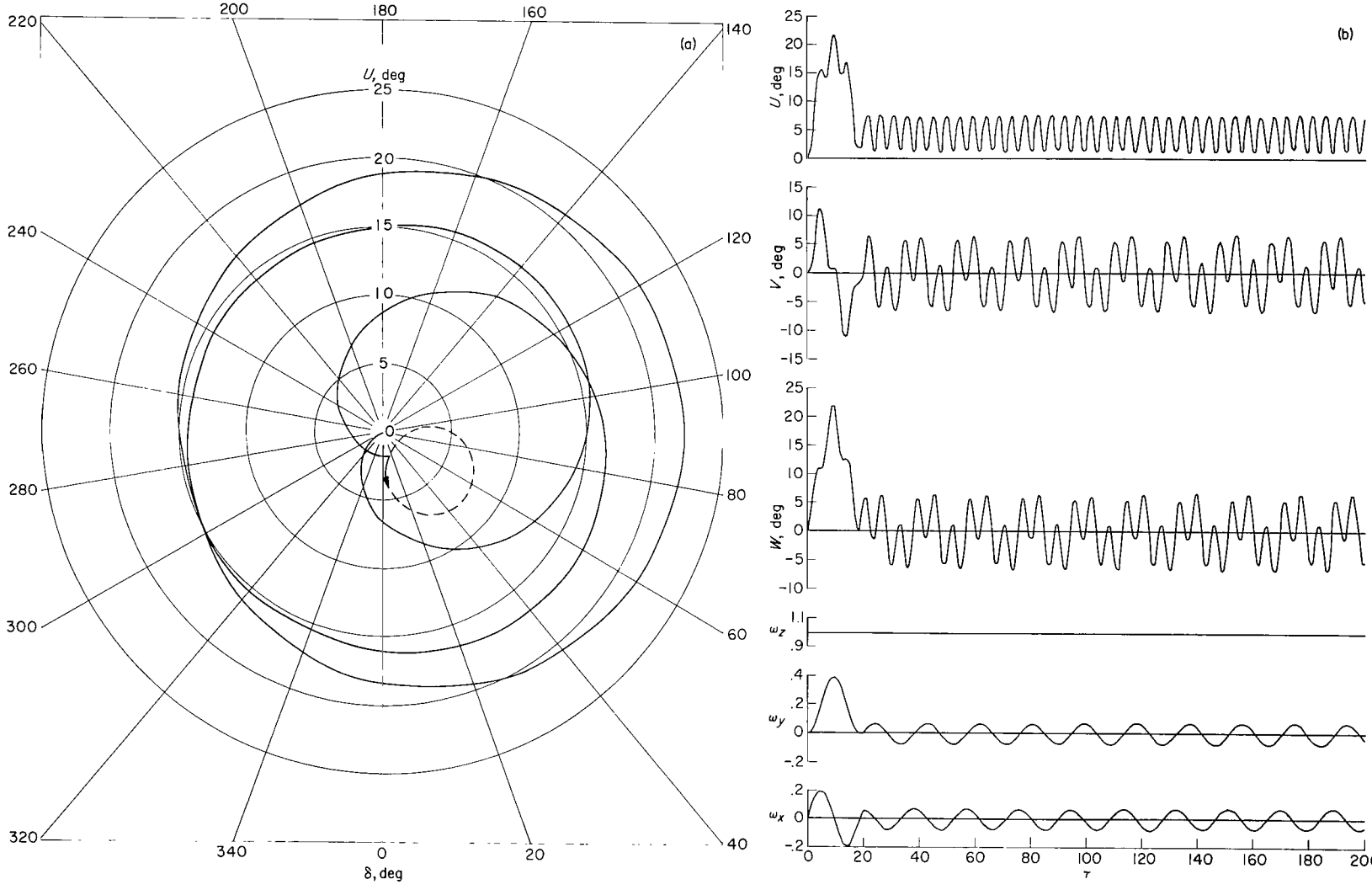

(a) Symmetry-axis trace.

(b) Time history.

Figure 2.- Motion of example station for an applied moment.

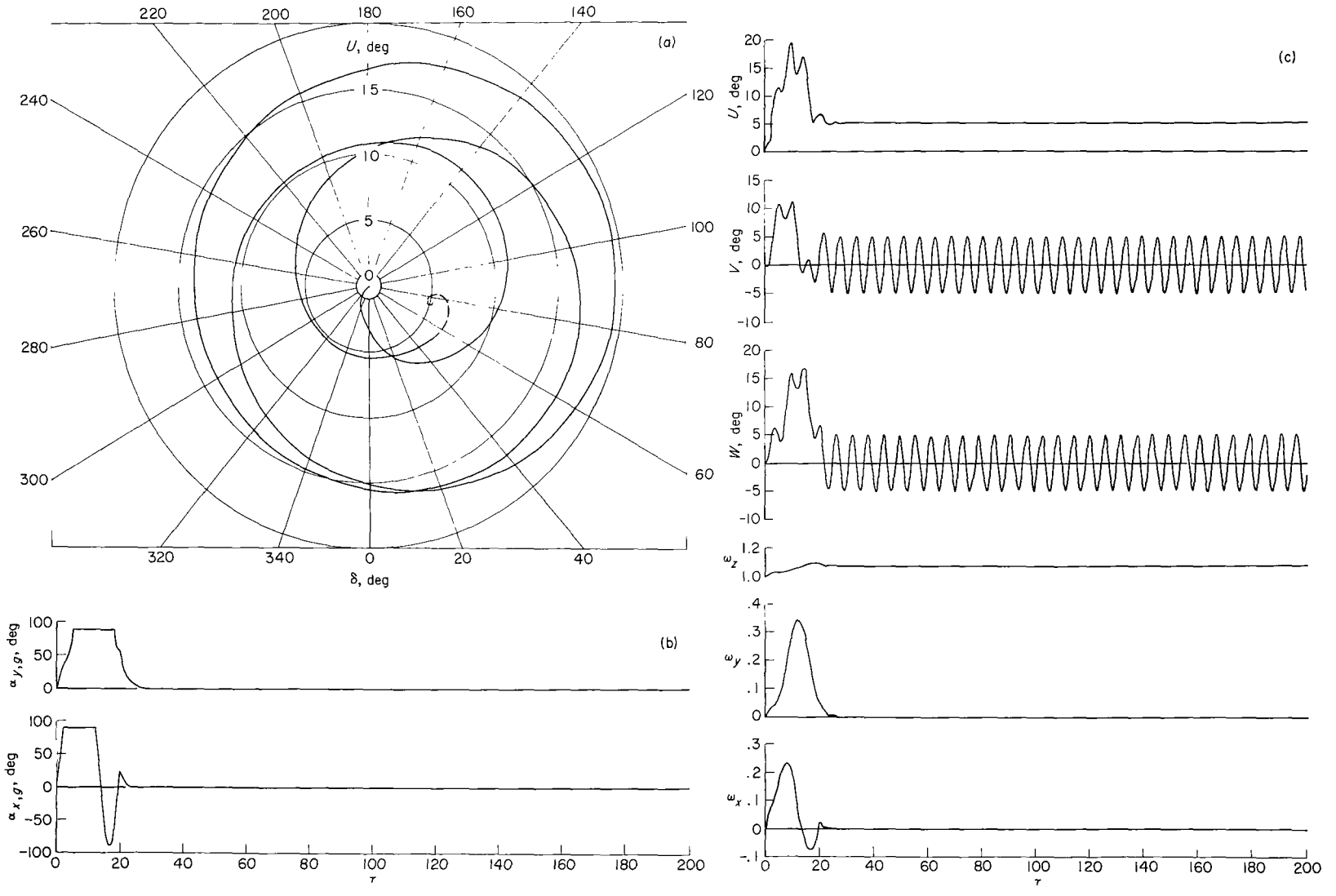

(a) Symmetry-axis trace.

(b) Gimbal angles.

(c) Time history.

Figure 3.- Motion of example station for an applied moment with a gyroscopic stability system.

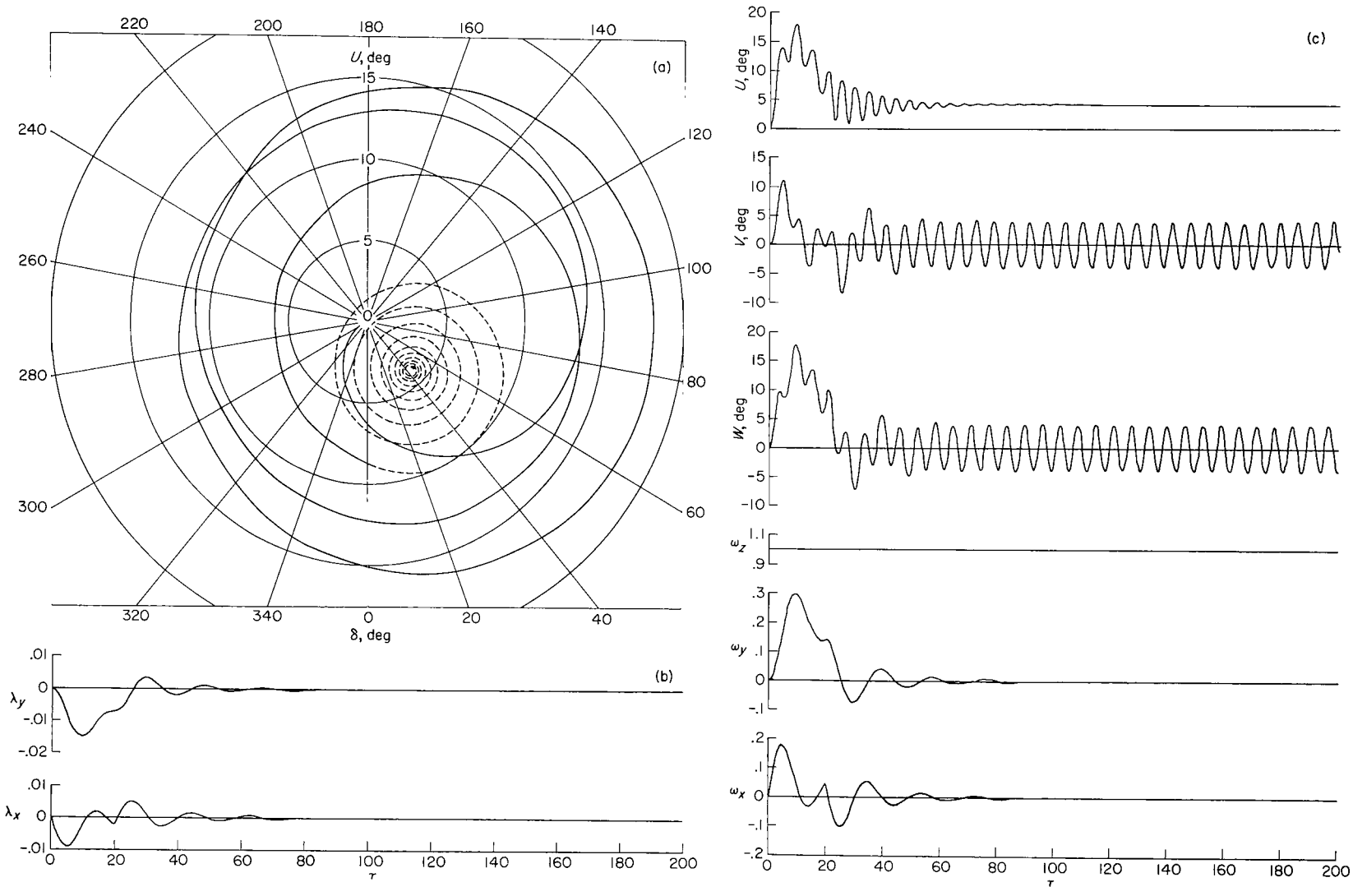

(a) Symmetry-axis trace.

(b) Damping moments.

(c) Time history.

Figure 4.- Motion of example station for an applied moment with a jet stability system.

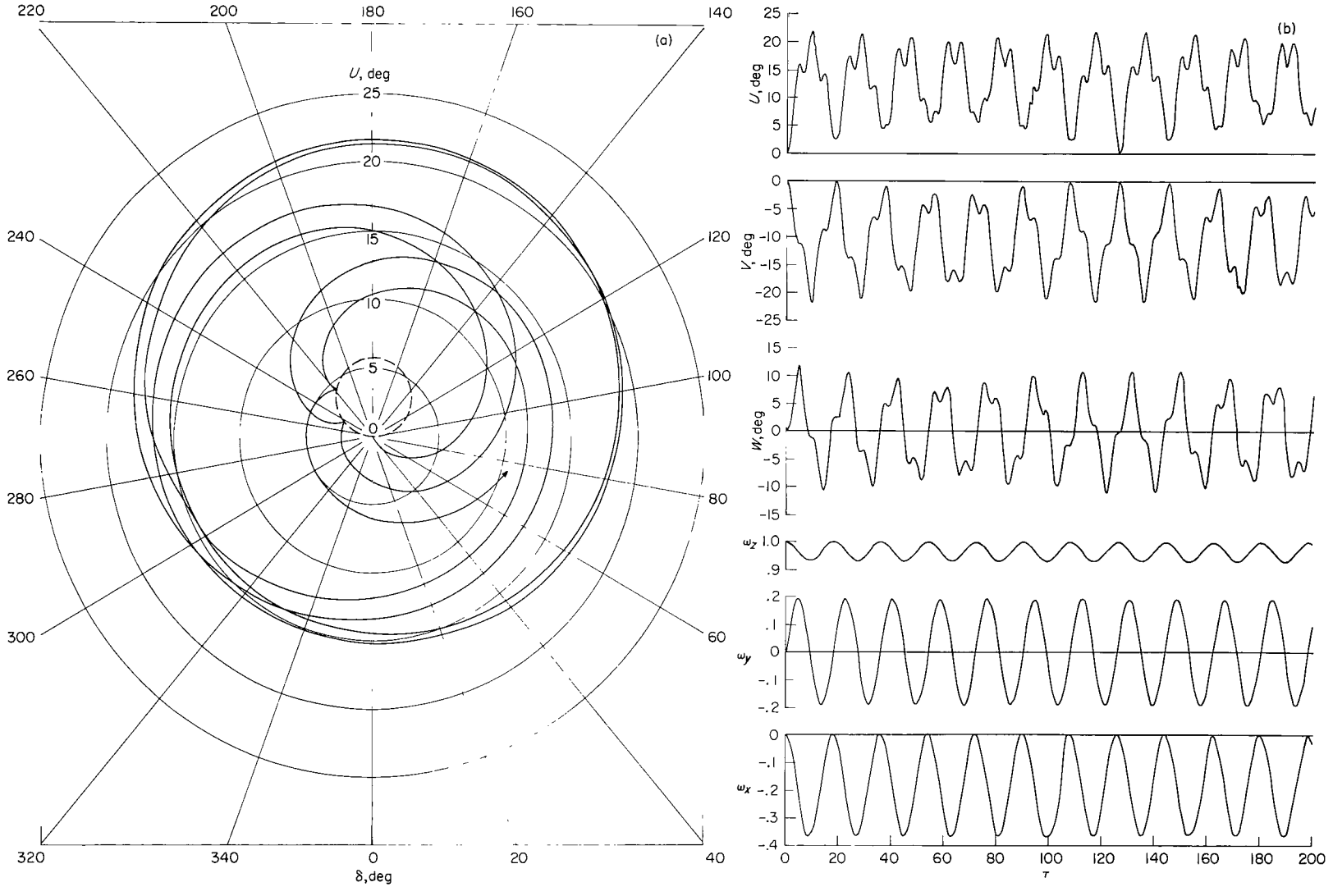

(a) Symmetry-axis trace.

(b) Time history.

Figure 5.- Motion of example station for a static product-of-inertia disturbance.

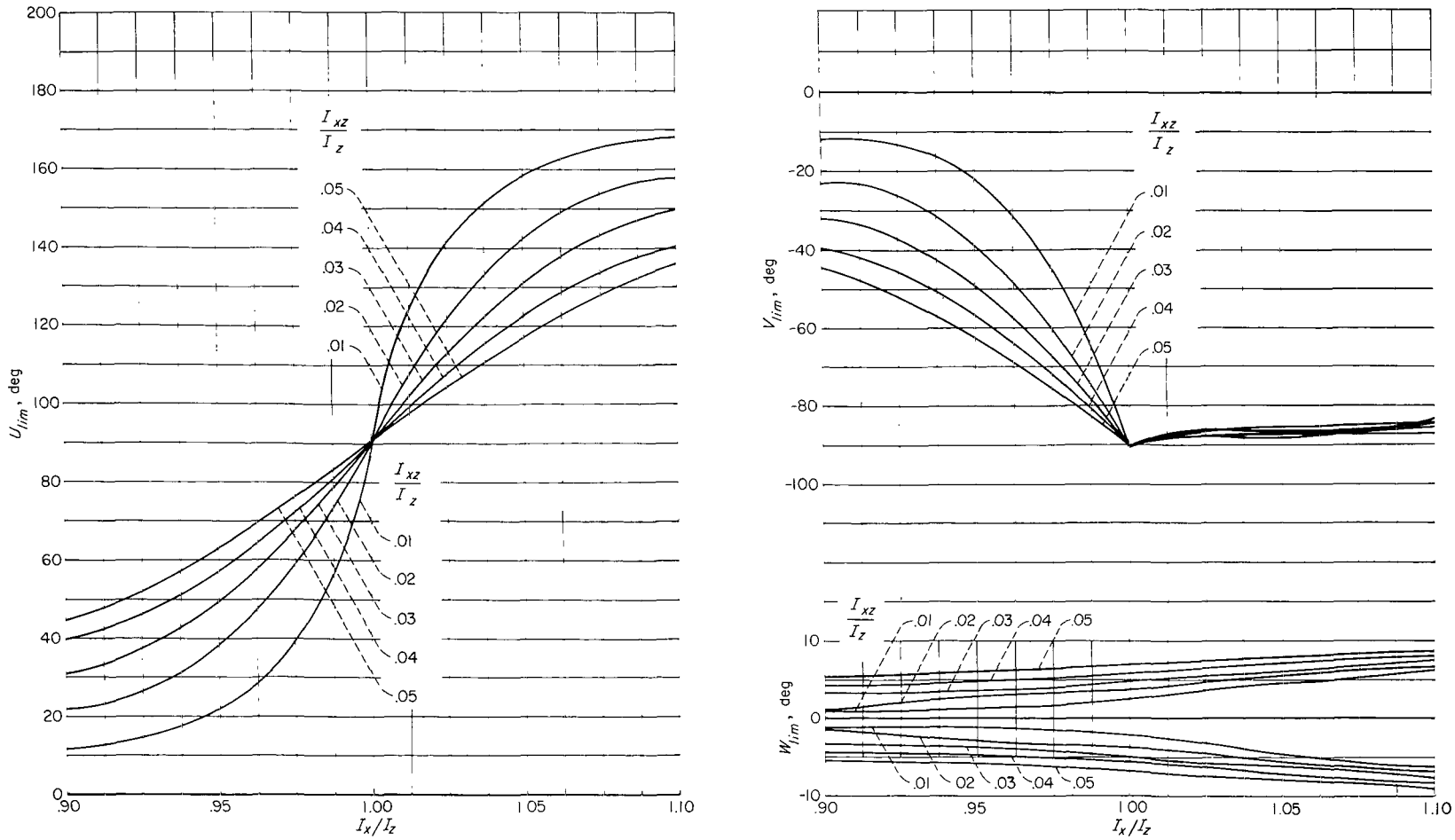

Figure 6.- Limit magnitudes of stability angles for various product-of-inertia disturbances and I_y/I_z = 0.1.

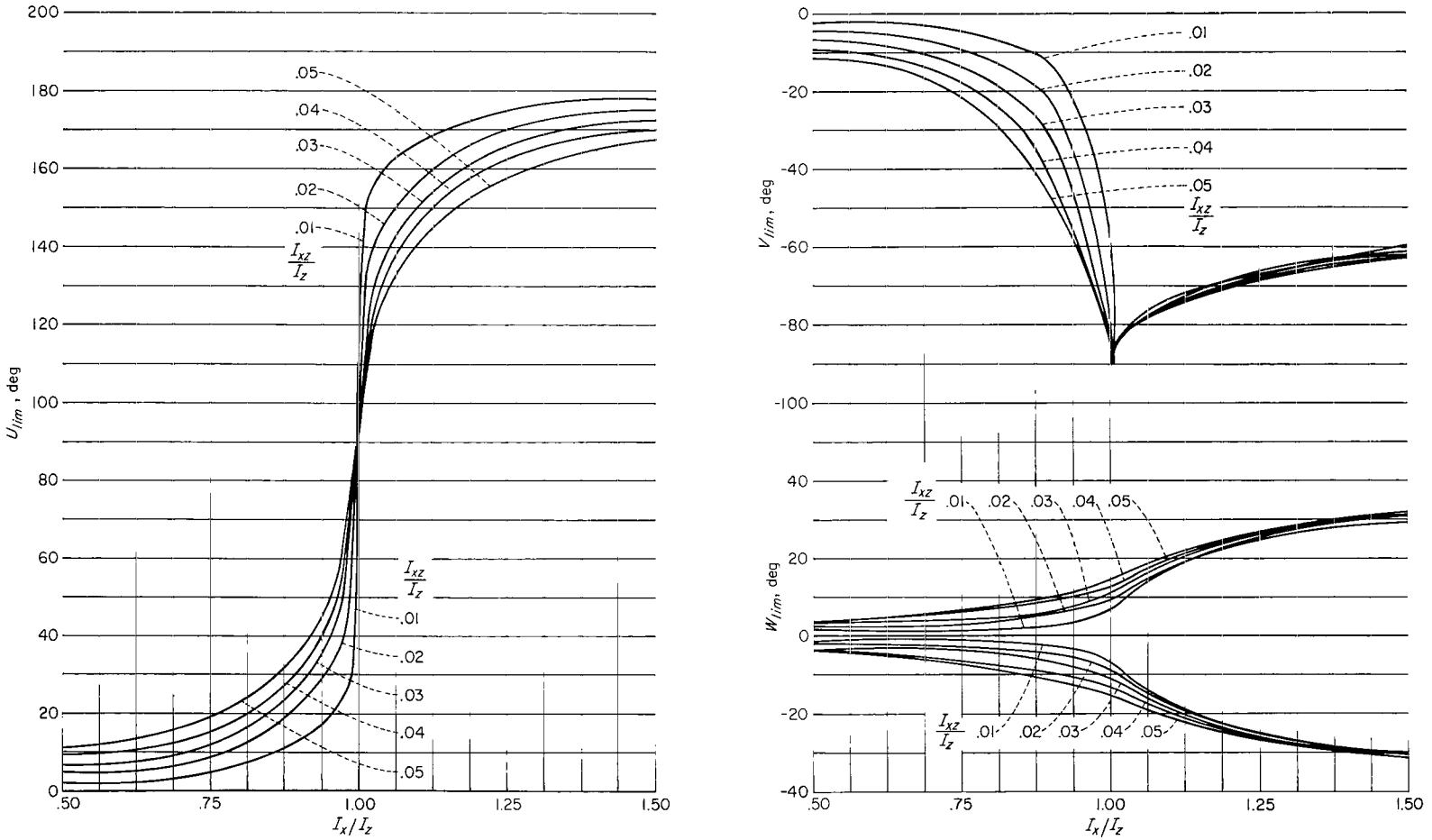

Figure 7.- Limit magnitudes of stability angles for various product-of-inertia disturbances and $I_y/I_z = 0.5$.

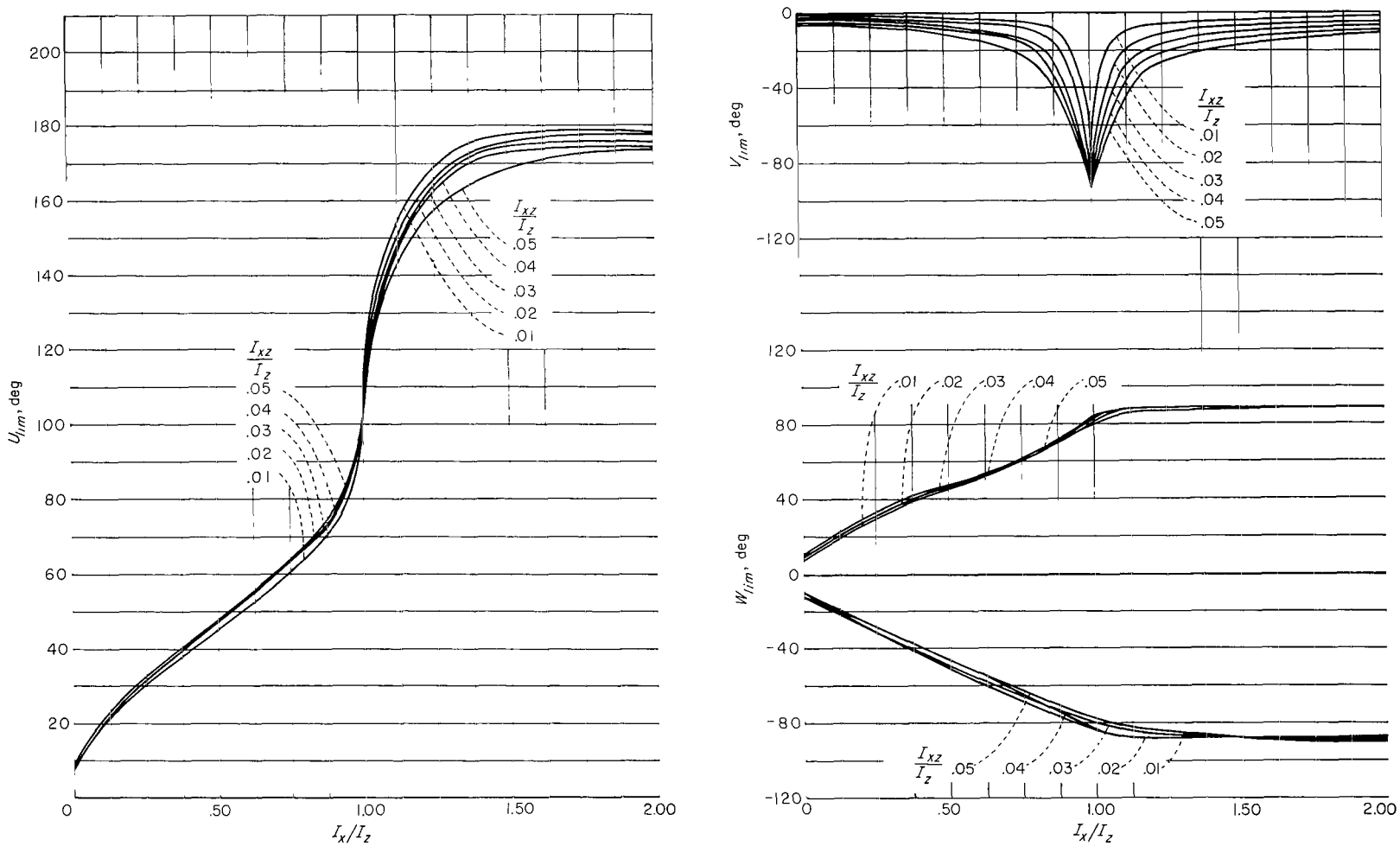

Figure 8.- Limit magnitudes of stability angles for various product-of-inertia disturbances and $I_y/I_z = 1.0$.

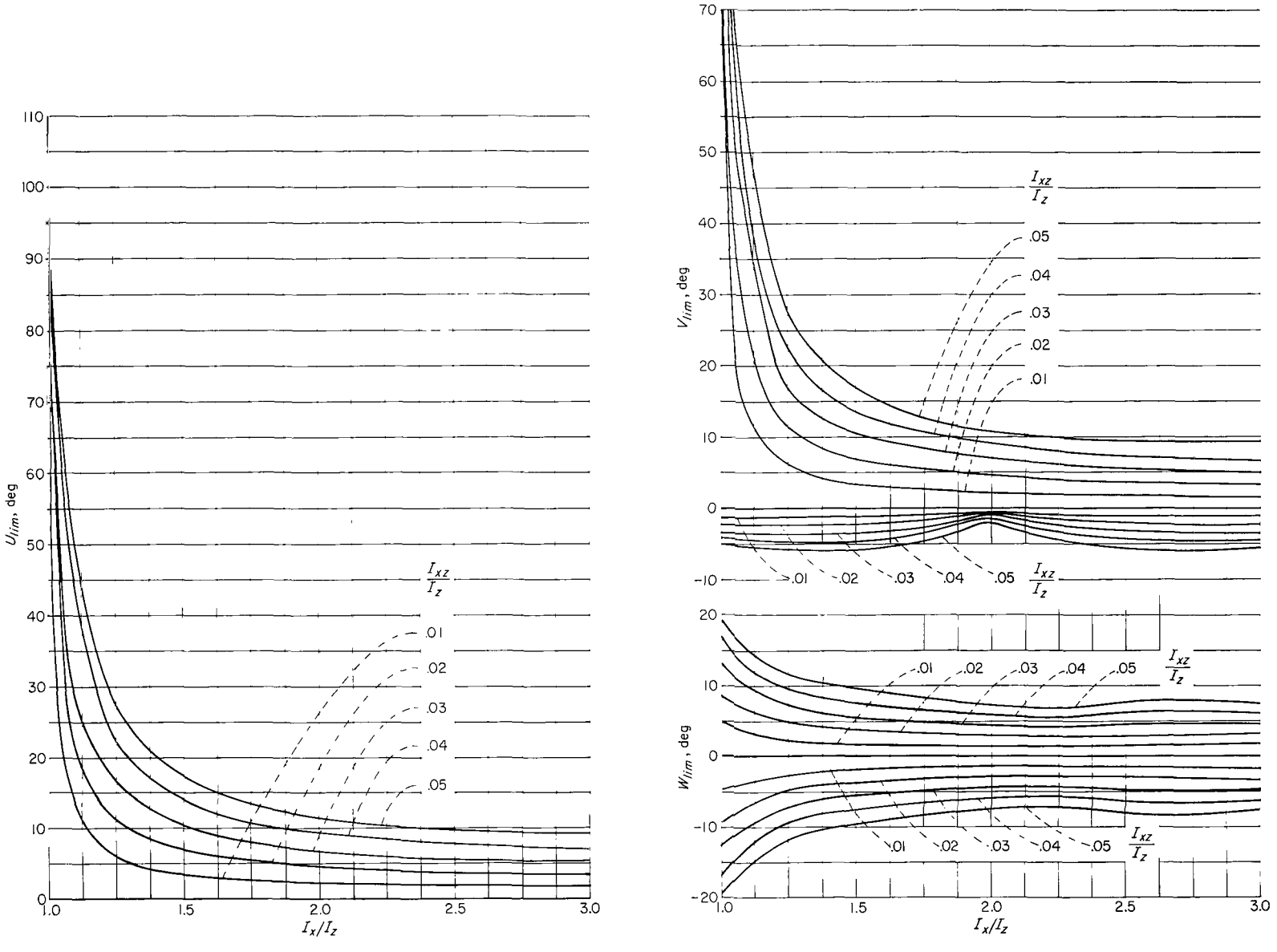

Figure 9.- Limit magnitudes of stability angles for various product-of-inertia disturbances and $I_y/I_z = 2.0$.

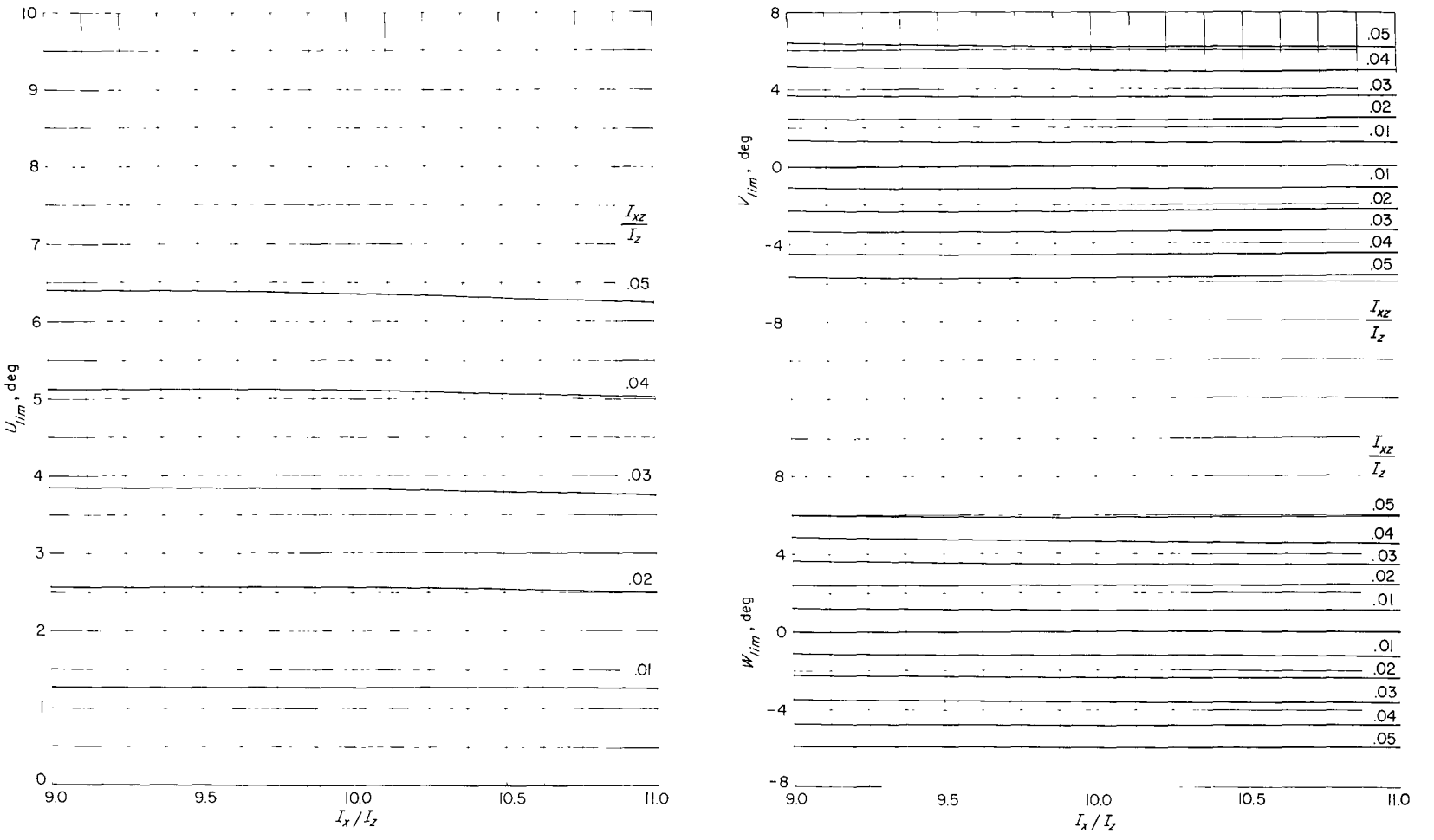

Figure 10.- Limit magnitudes of stability angles for various product-of-inertia disturbances and $I_y/I_z = 10.0$.

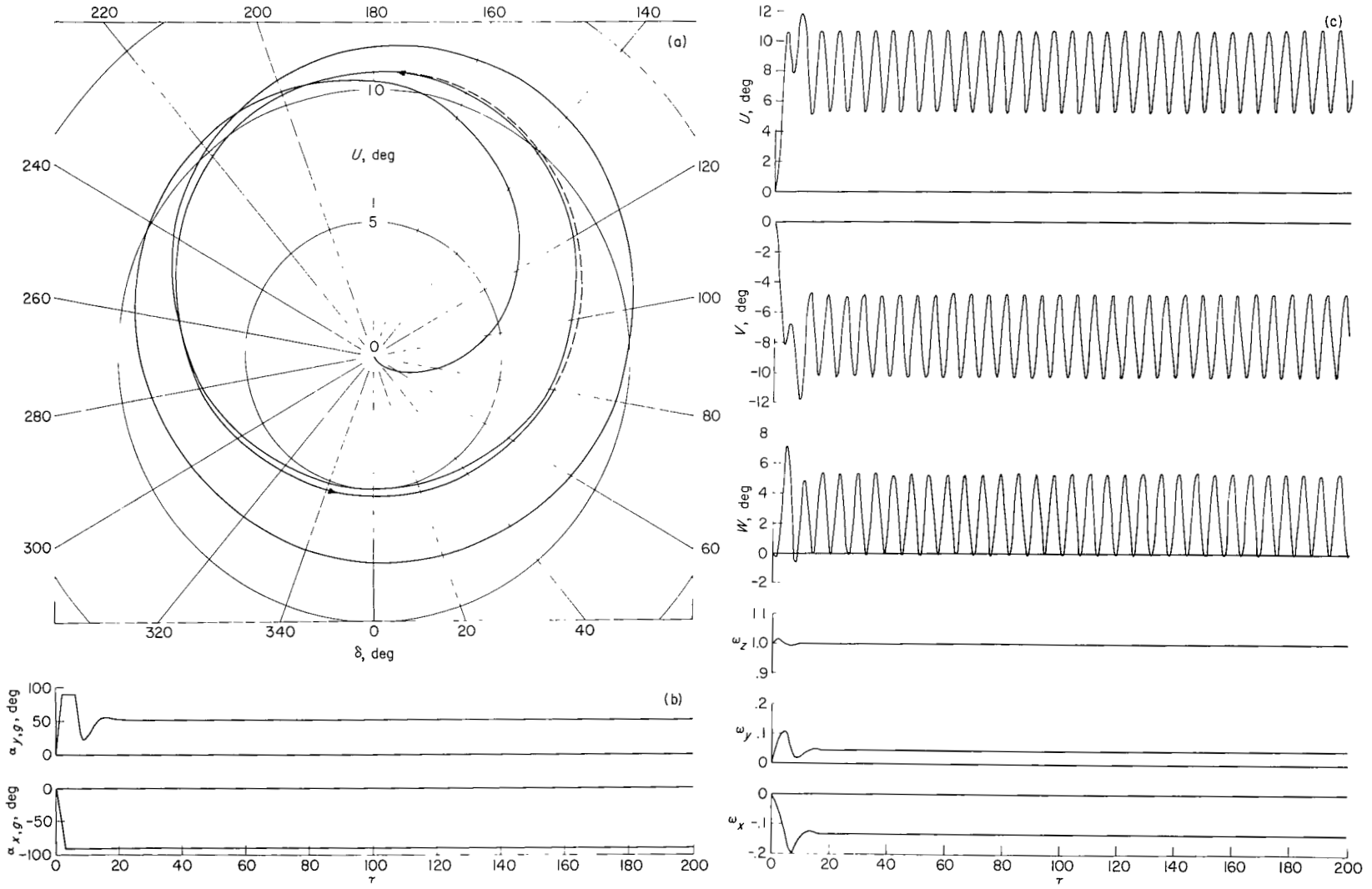

(a) Symmetry-axis trace.

(b) Gimbal angles.

(c) Time history.

Figure 11.- Motion of example station for a static product-of-inertia disturbance with a gyroscopic stability system.

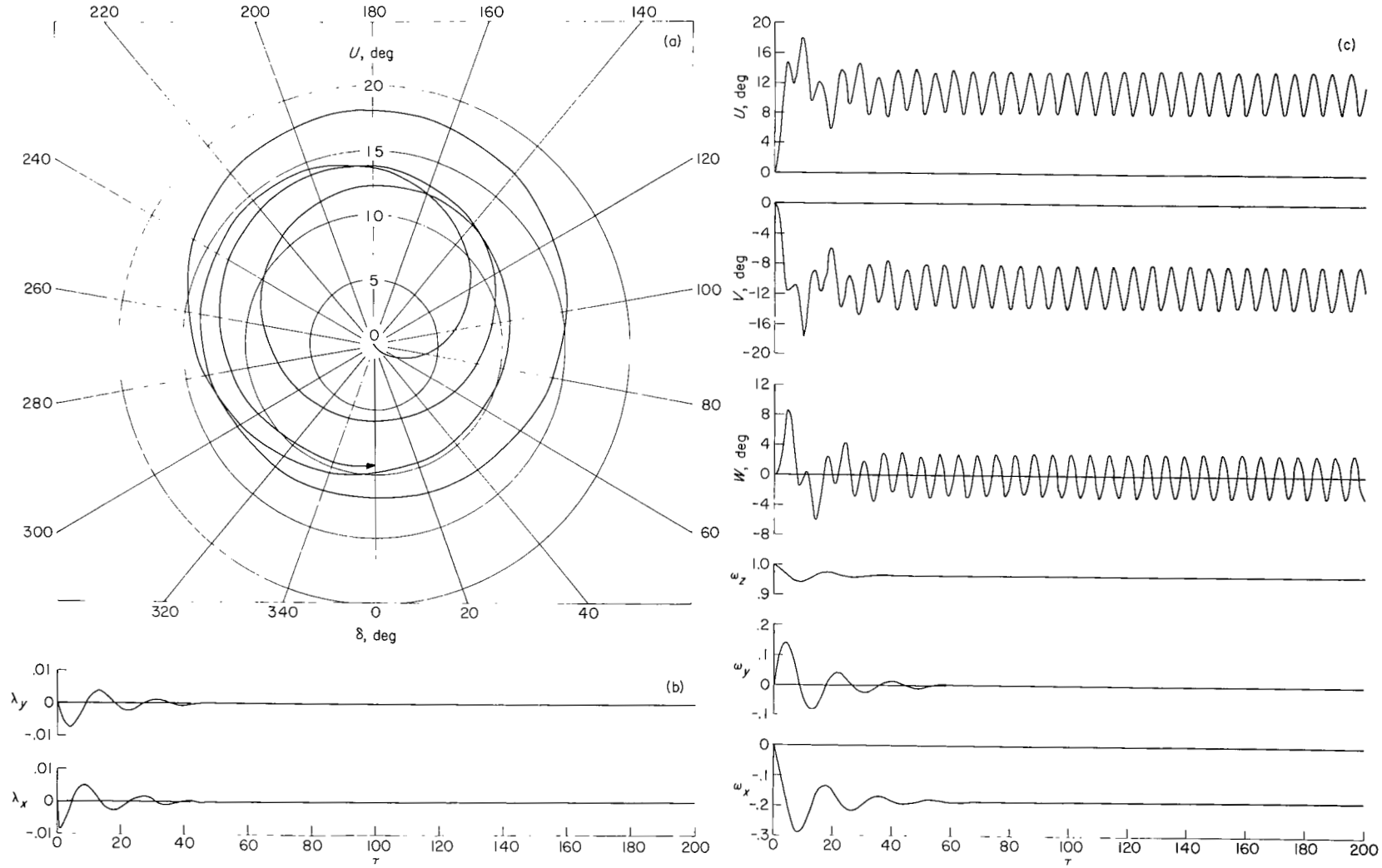

(a) Symmetry-axis trace.

(b) Damping moments.

(c) Time history.

Figure 12.- Motion of example station for a static product-of-inertia disturbance with a jet stability system.

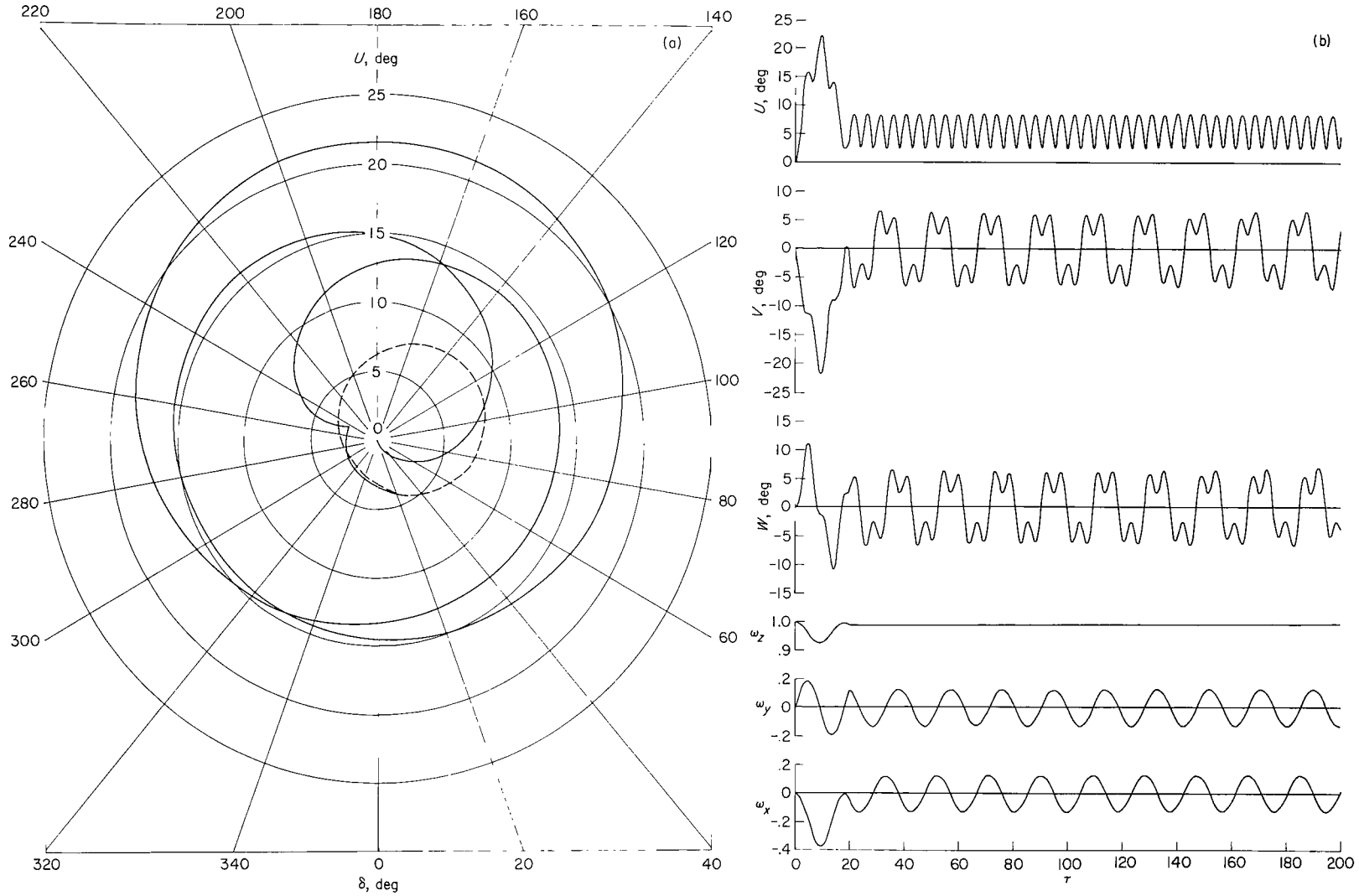

(a) Symmetry-axis trace.

(b) Time history.

Figure 13.- Motion of example station for a temporary static product-of-inertia disturbance.

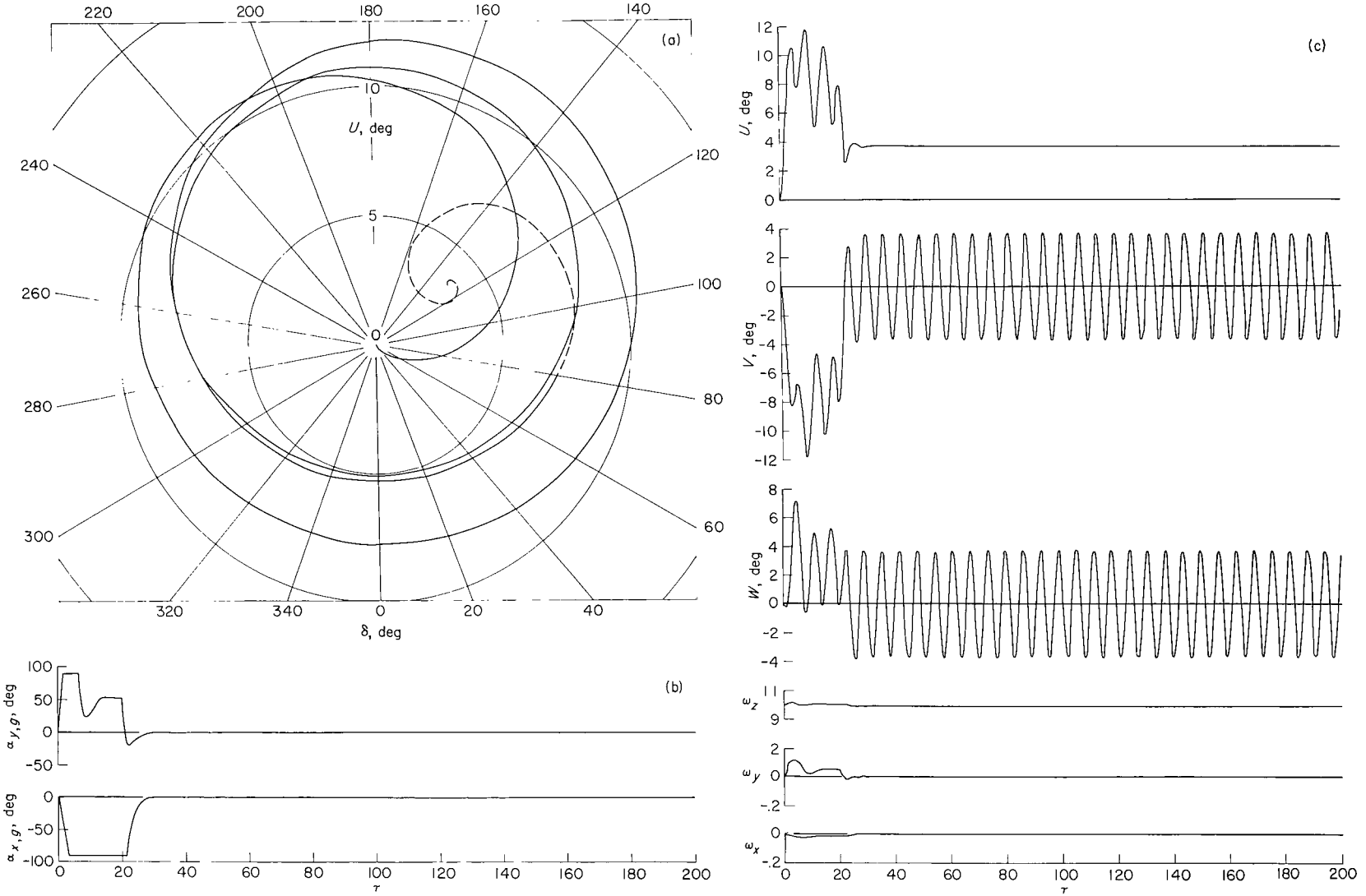

(a) Symmetry-axis trace.

(b) Gimbal angles.

(c) Time history.

Figure 14.- Motion of example station for a temporary static product-of-inertia disturbance with a gyroscopic stability system.

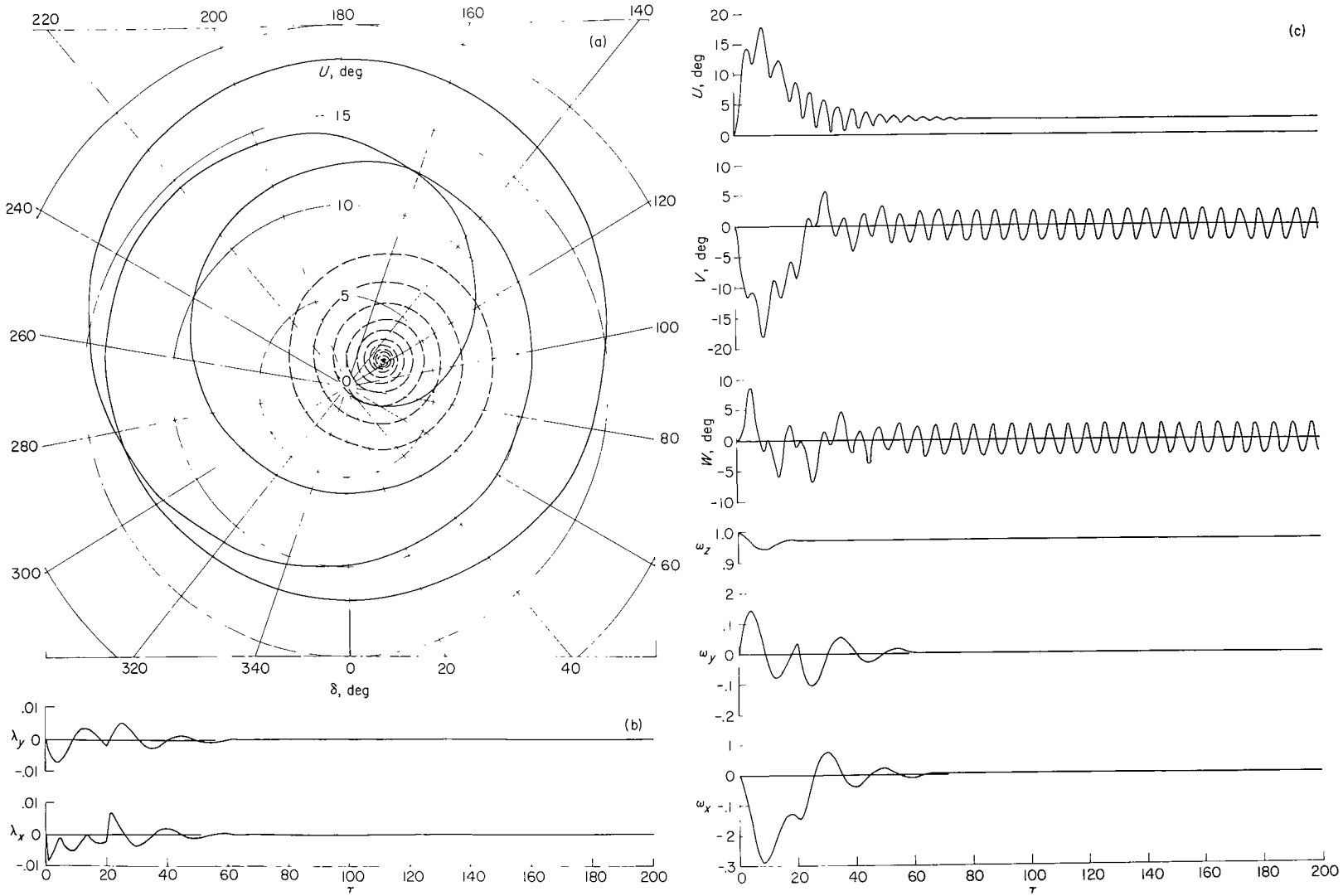

(a) Symmetry-axis trace.

(b) Damping moments.

(c) Time history.

Figure 15.- Motion of example station for a temporary static product-of-inertia disturbance with a jet stability system.

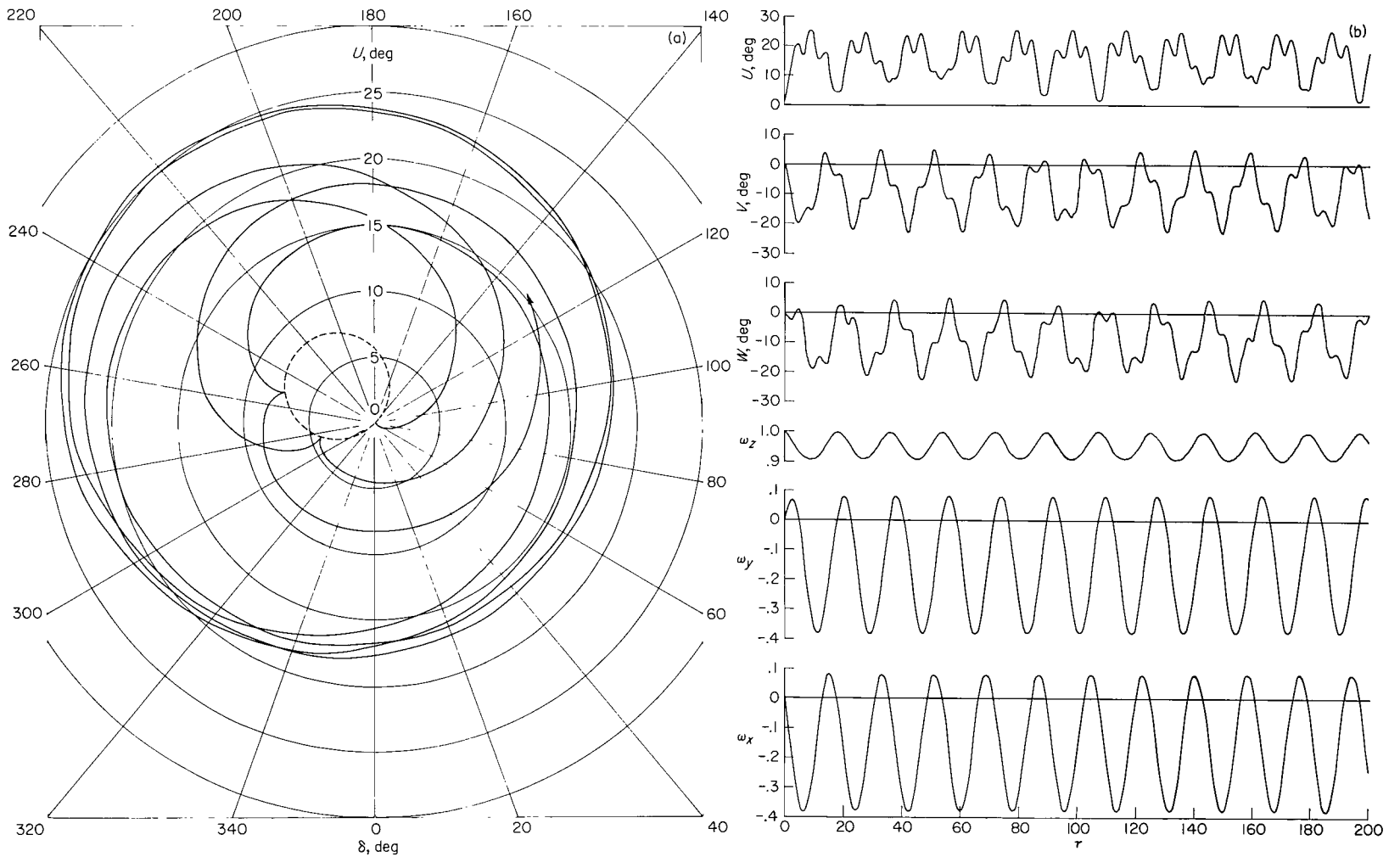

(a) Symmetry-axis trace.

(b) Time history.

Figure 16.- Motion of example station for a combined static product-of-inertia disturbance.

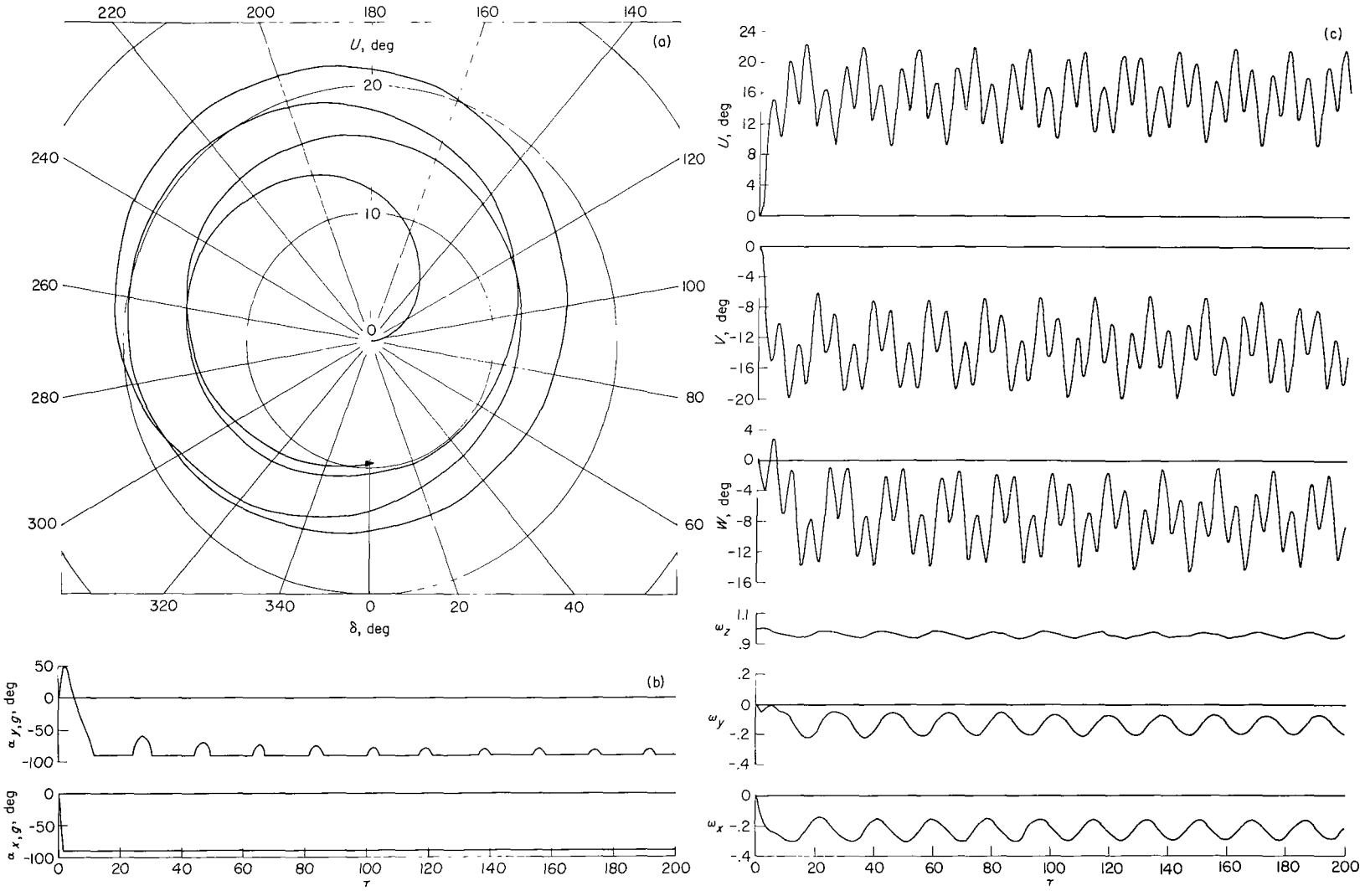

(a) Symmetry-axis trace.

(b) Gimbal angles.

(c) Time history.

Figure 17.- Motion of example station for a combined static product-of-inertia disturbance with a gyroscopic stability system.

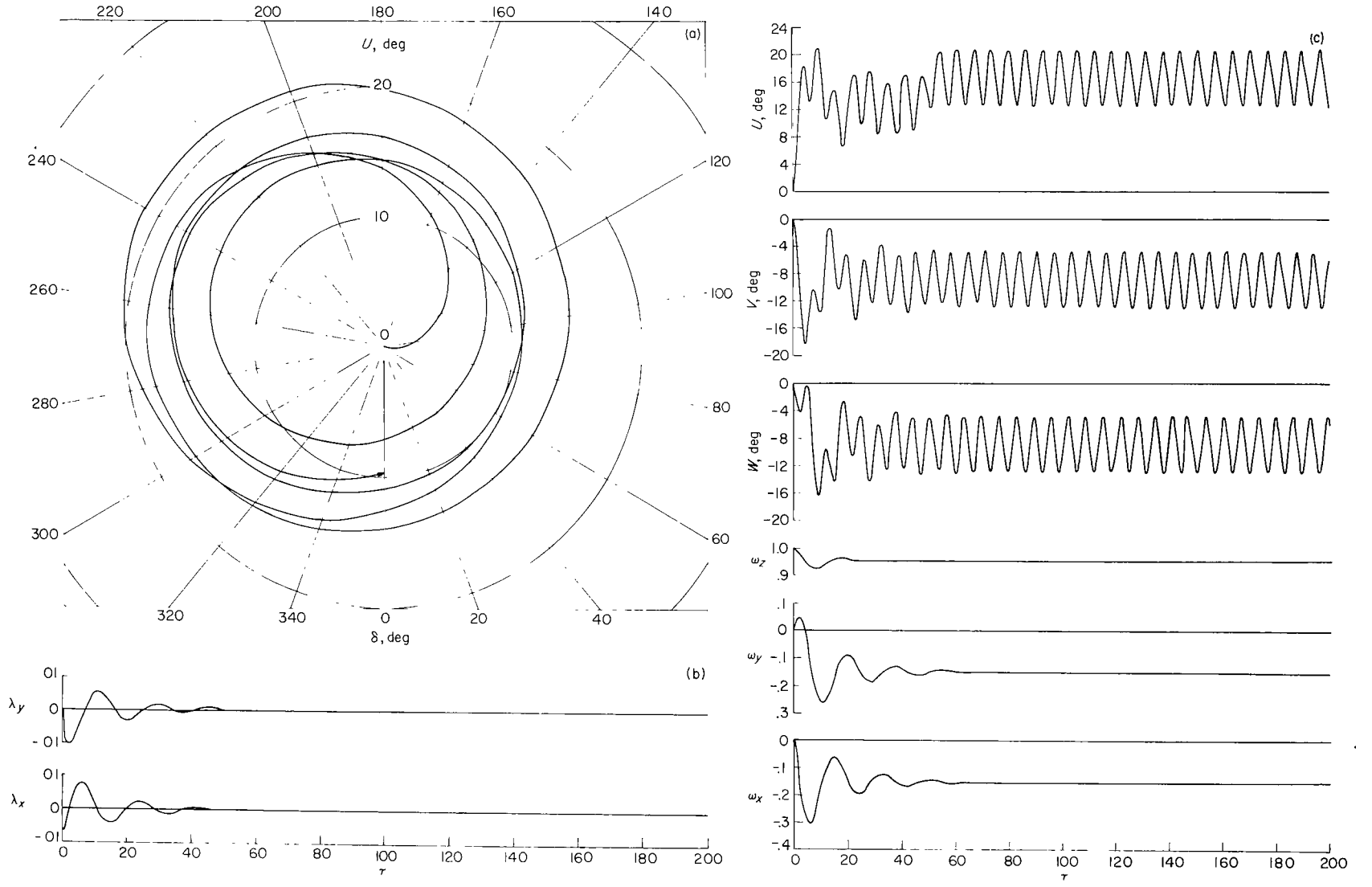

(a) Symmetry-axis trace.

(b) Damping moments.

(c) Time history.

Figure 18.- Motion of example station for a combined static product-of-inertia disturbance with a jet stability system.

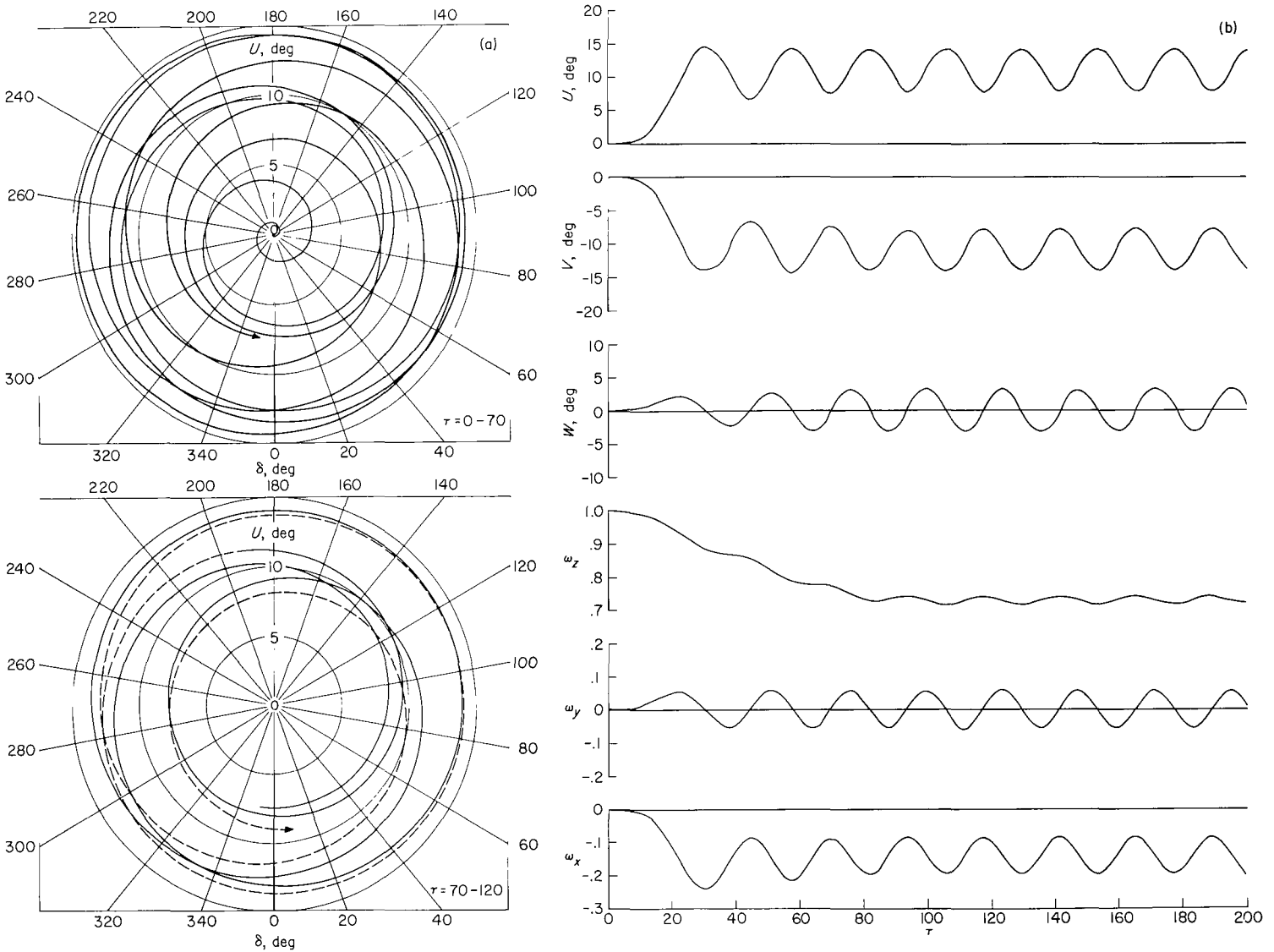

(a) Symmetry-axis trace.

(b) Time history.

Figure 19.- Motion of example station for a transient radial product-of-inertia disturbance and T = 100.

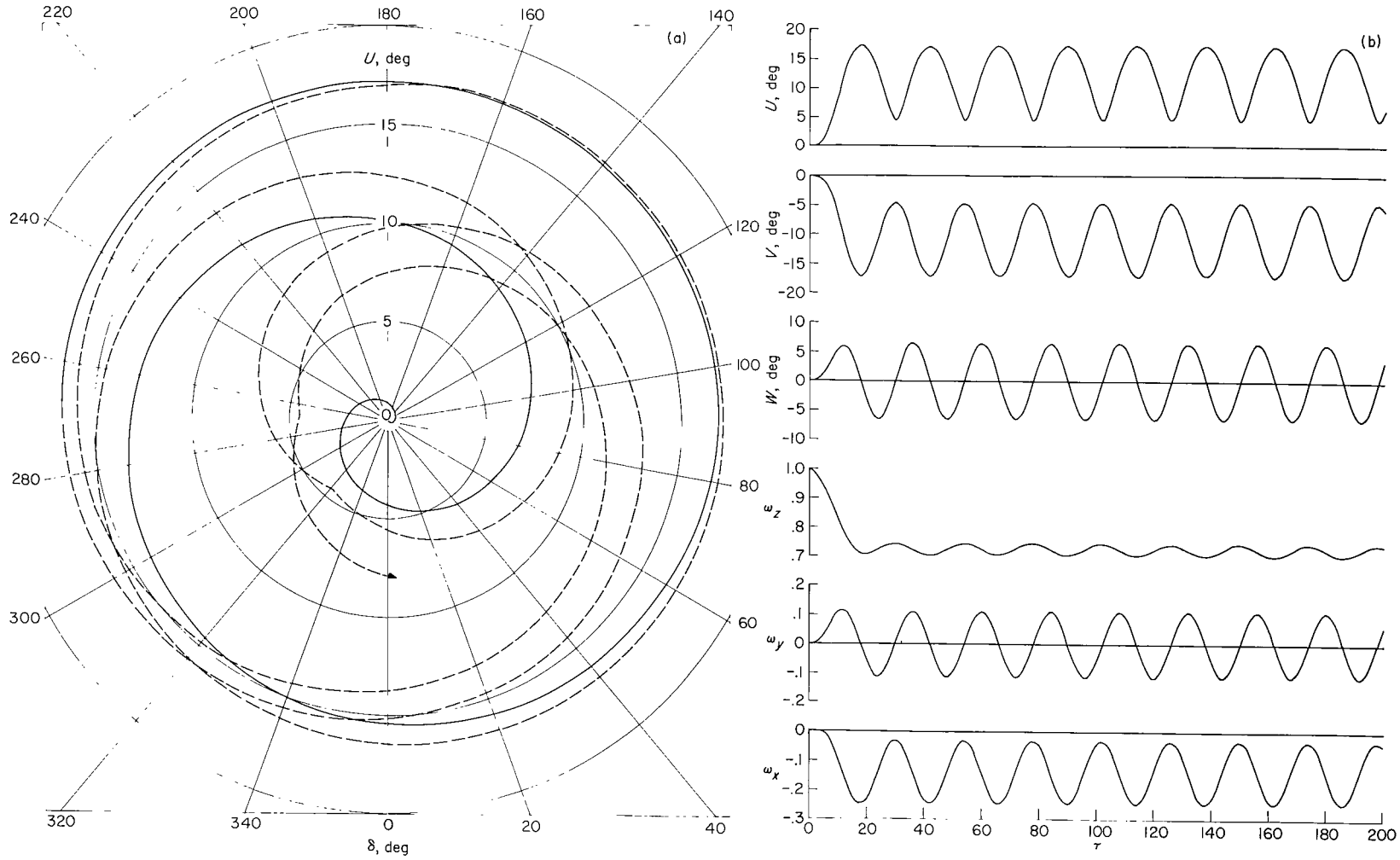

(a) Symmetry-axis trace.

(b) Time history.

Figure 20.- Motion of example station for a transient radial product-of-inertia disturbance and T = 20.

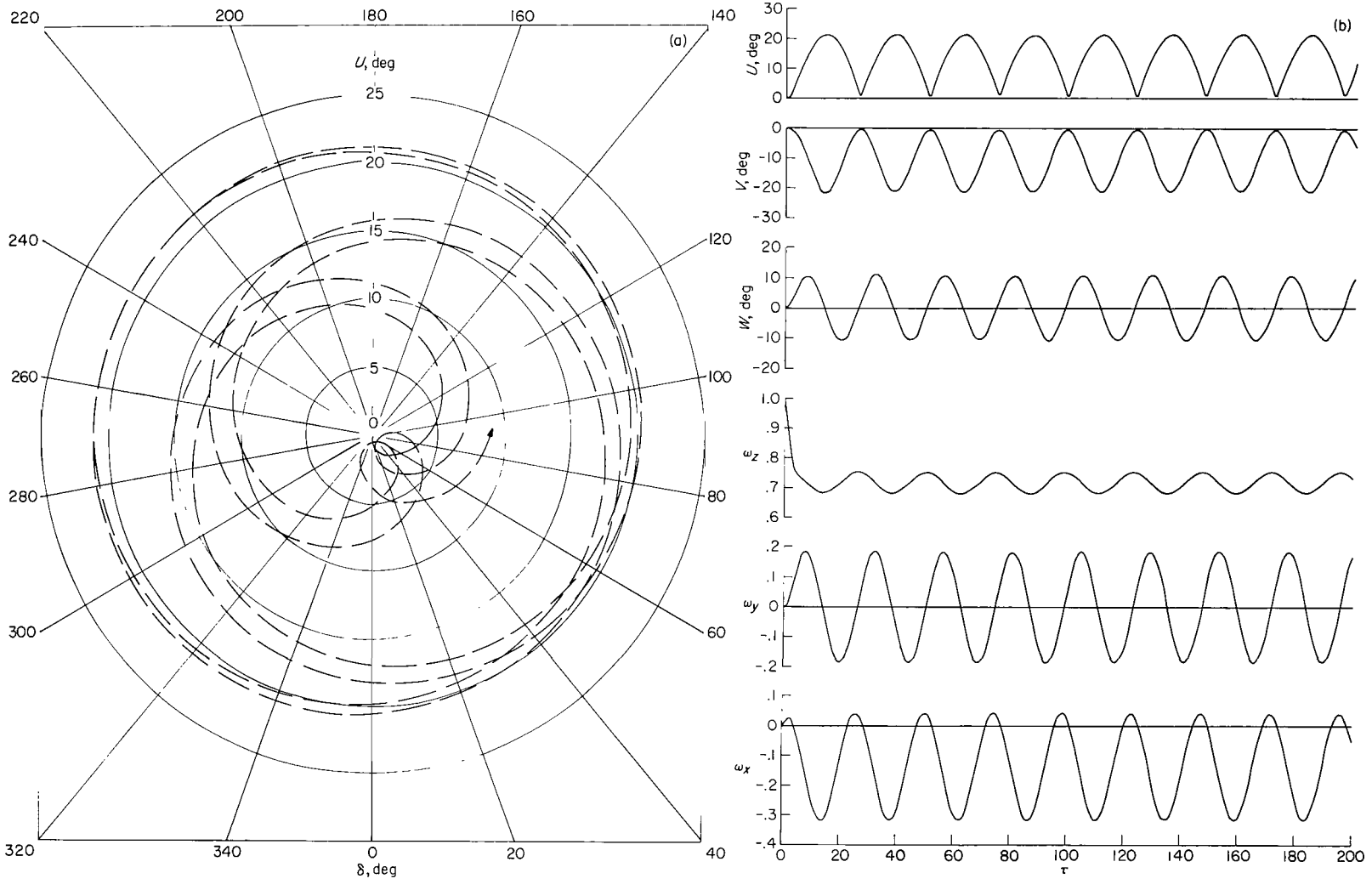

(a) Symmetry-axis trace.

(b) Time history.

Figure 21.- Motion of example station for a transient radial product-of-inertia disturbance and $T = 4$.

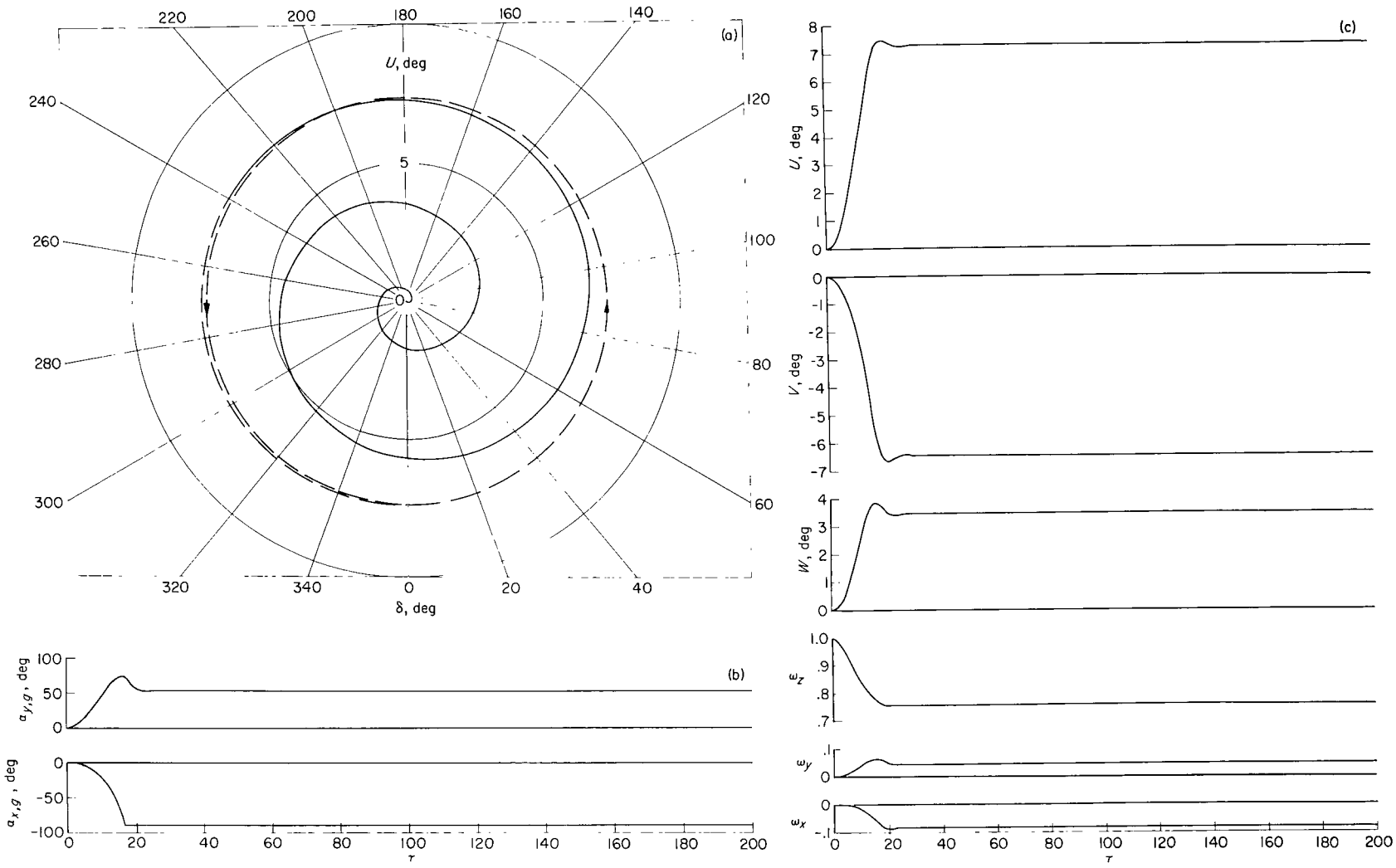

(a) Symmetry-axis trace.

(b) Gimbal angles.

(c) Time history.

Figure 22.- Motion of example station for a transient radial product-of-inertia disturbance and T = 20 with a gyroscopic stability system.

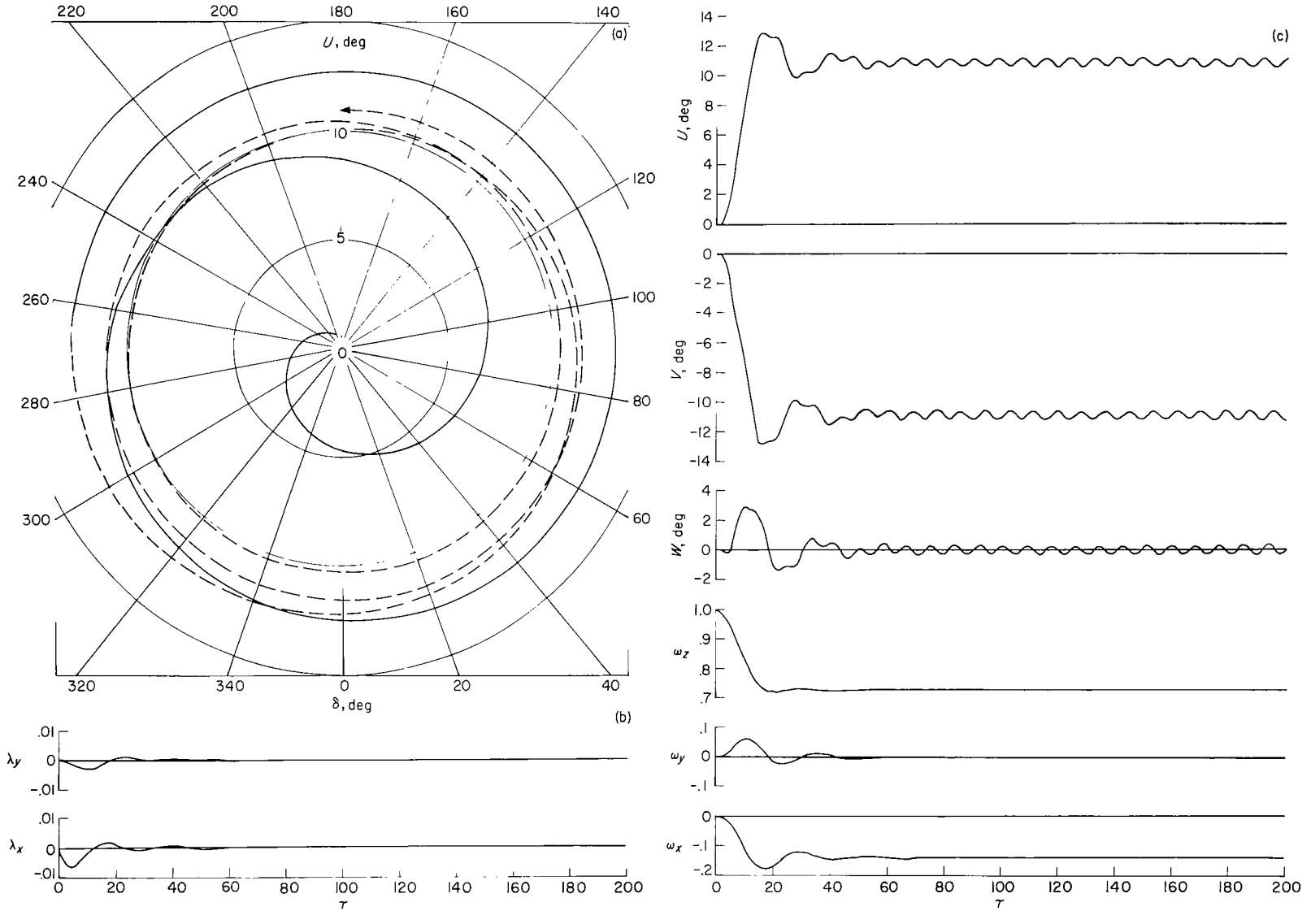

(a) Symmetry-axis trace.

(b) Damping moments.

(c) Time history.

Figure 23.- Motion of example station for a transient radial product-of-inertia disturbance and T = 20 with a jet stability system.

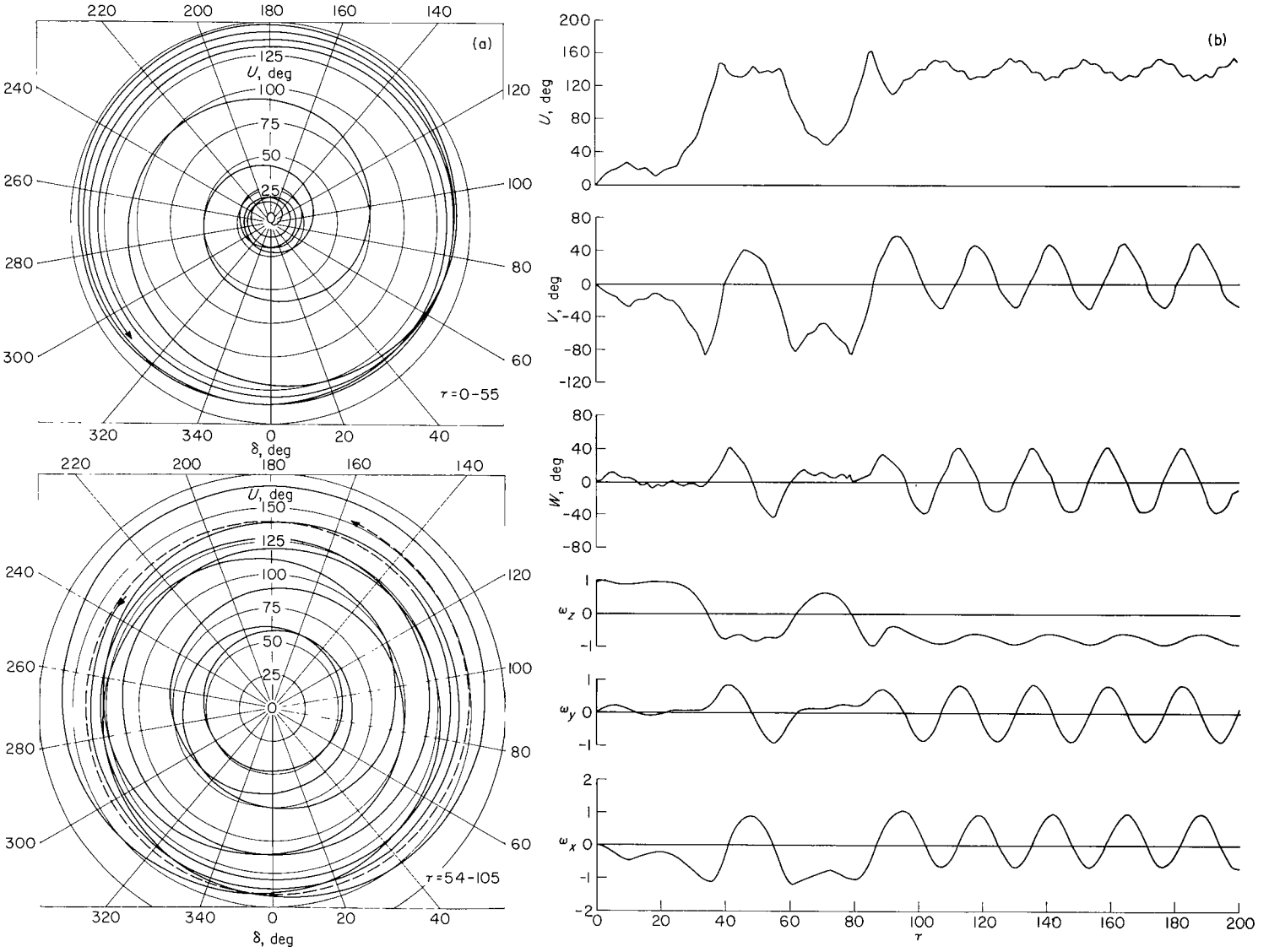

(a) Symmetry-axis trace.

(b) Time history.

Figure 24.- Motion of example station for a transient tangential product-of-inertia disturbance and $\bar{T}$ = 100.

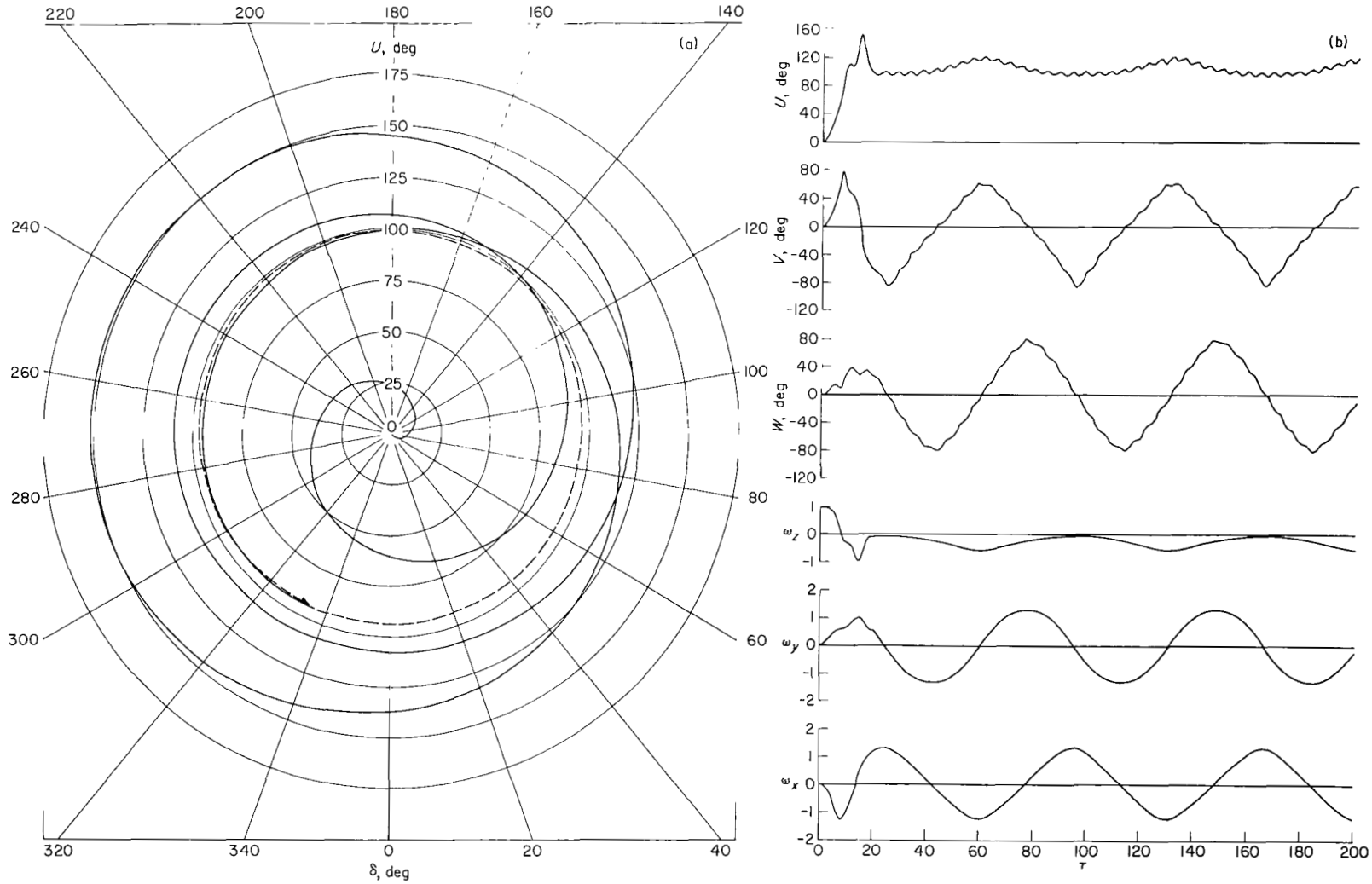

(a) Symmetry-axis trace.

(b) Time history.

Figure 25.- Motion of example station for a transient tangential product-of-inertia disturbance and T = 20.

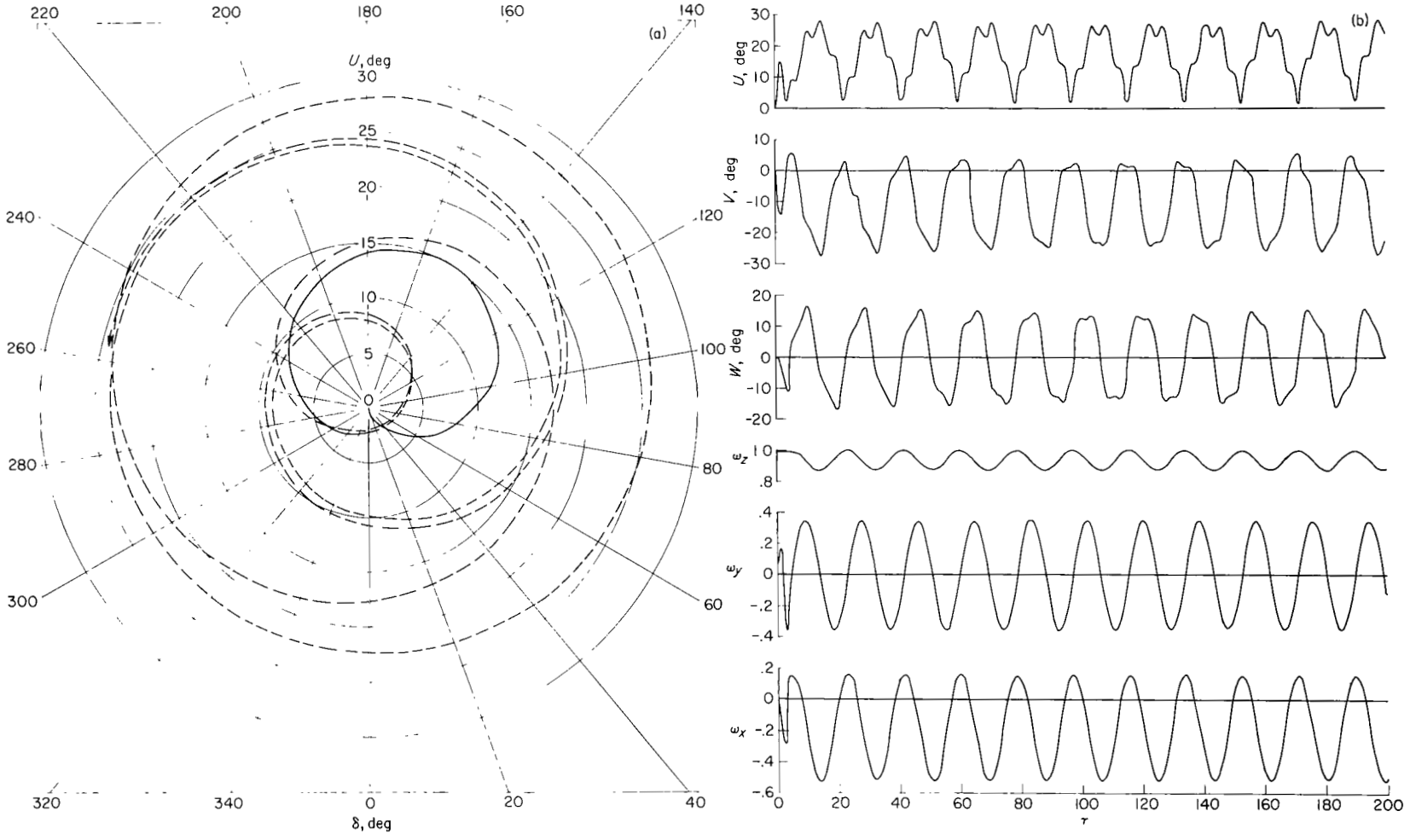

(a) Symmetry-axis trace.

(b) Time history.

Figure 26.- Motion of example station for a transient tangential product-of-inertia disturbance and T = 4.

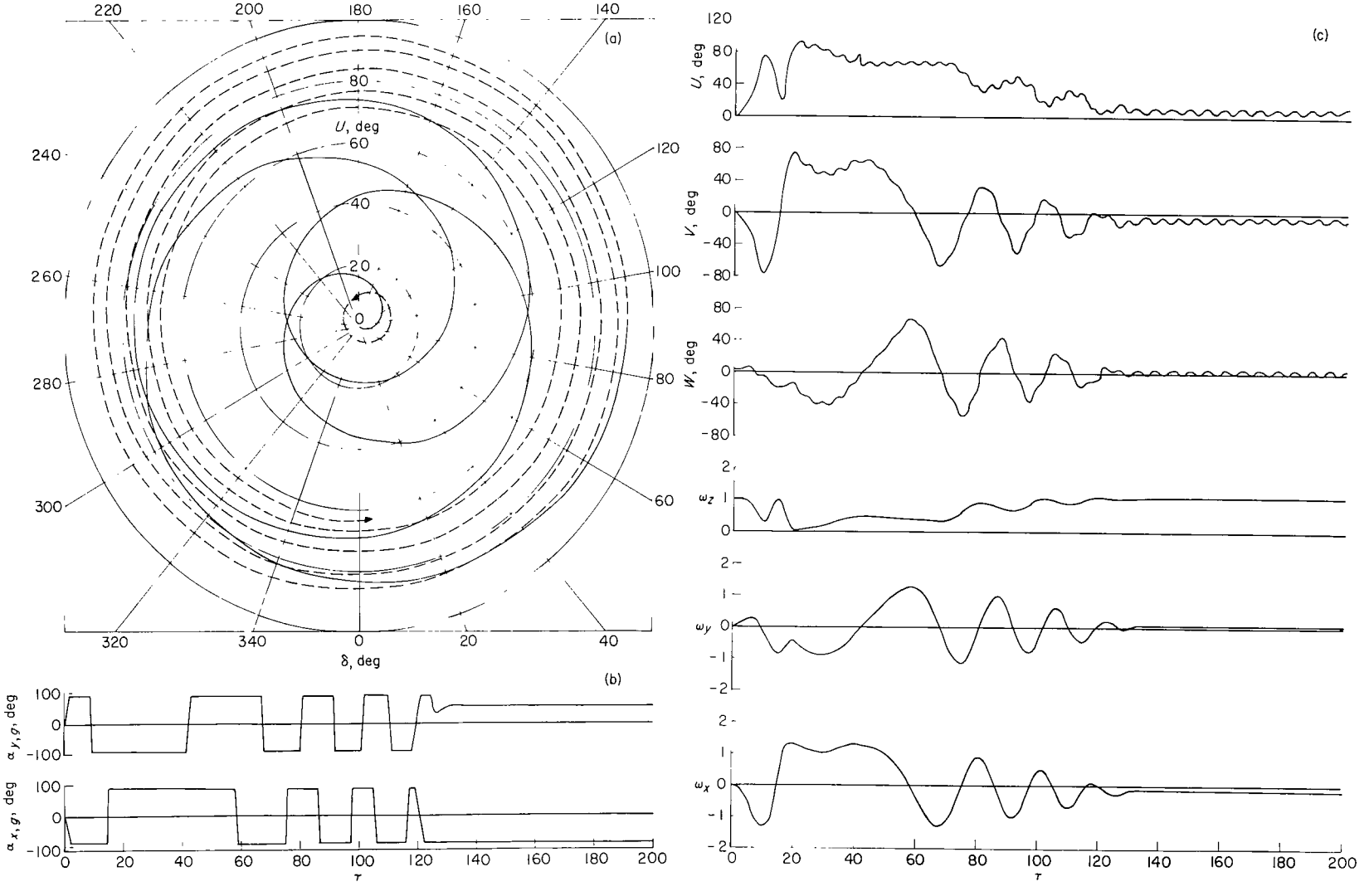

(a) Symmetry-axis trace.

(b) Gimbal angles.

(c) Time history.

Figure 27.- Motion of example station for a transient tangential product-of-inertia disturbance and T = 20 with a gyroscopic stability system.

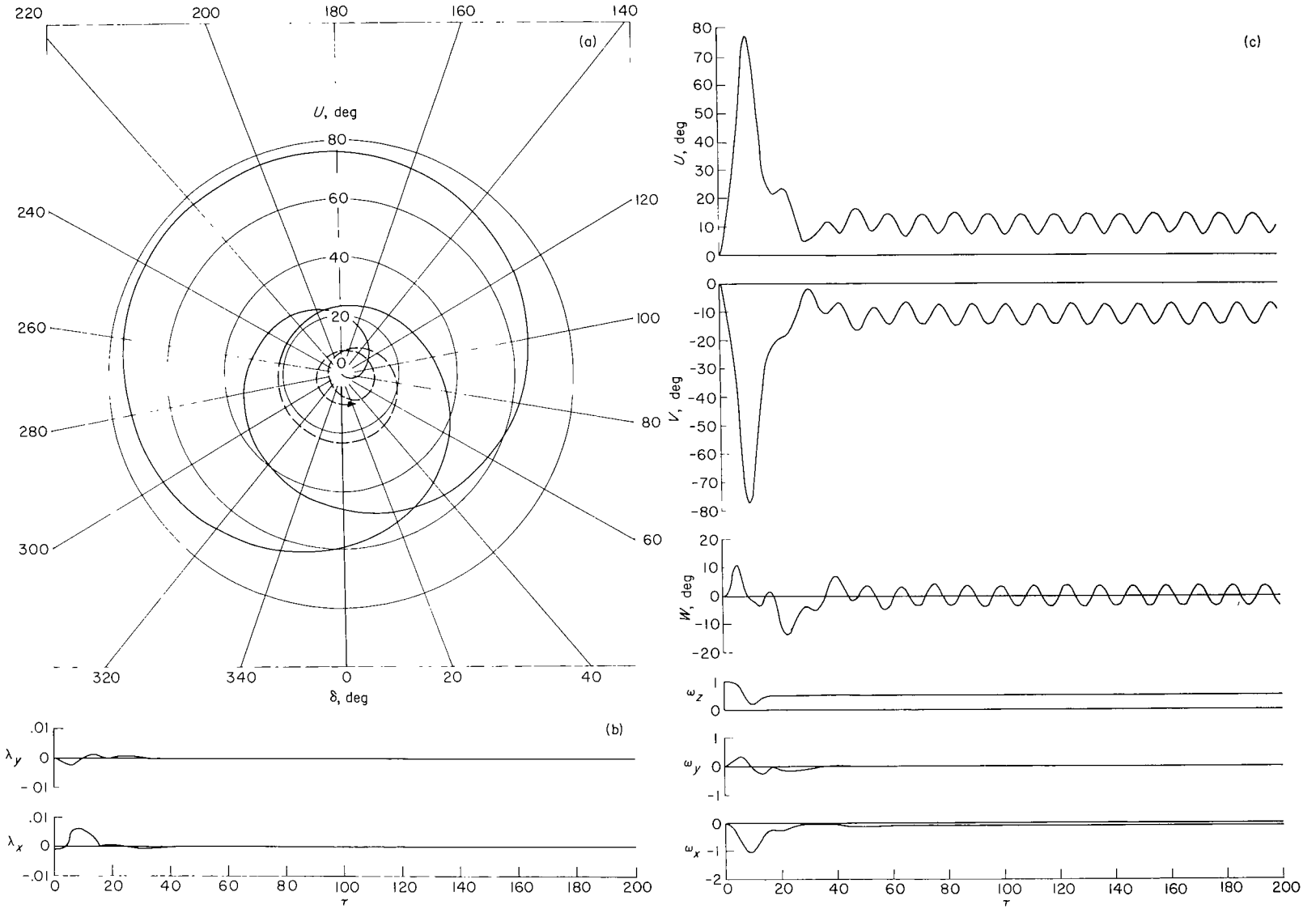

(a) Symmetry-axis trace.

(b) Damping moments.

(c) Time history.

Figure 28.- Motion of example station for a transient tangential product-of-inertia disturbance and T = 20 with a jet stability system.

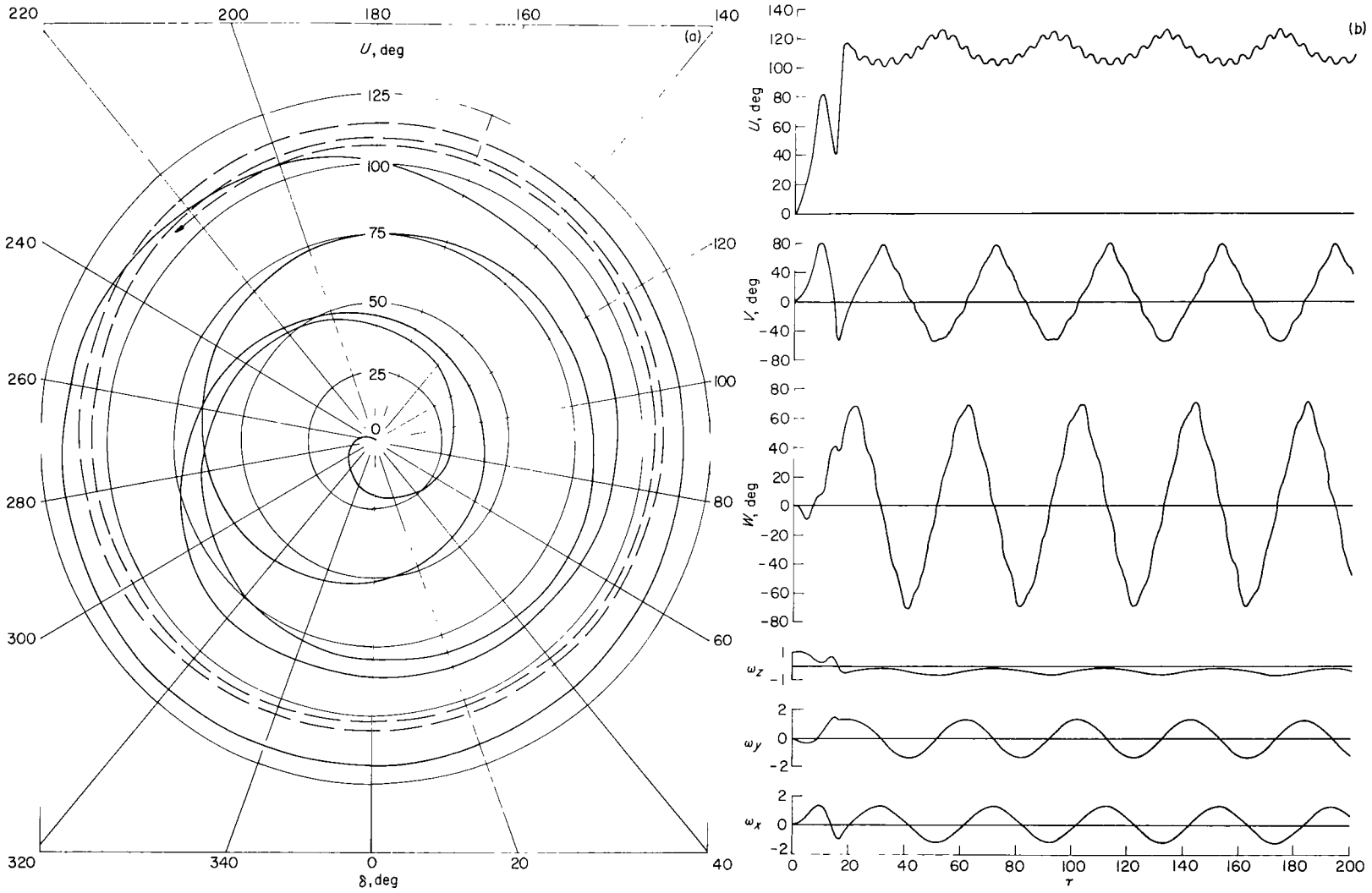

(a) Symmetry-axis trace.

(b) Time history.

Figure 29.- Motion of example station for a general transient product-of-inertia disturbance.

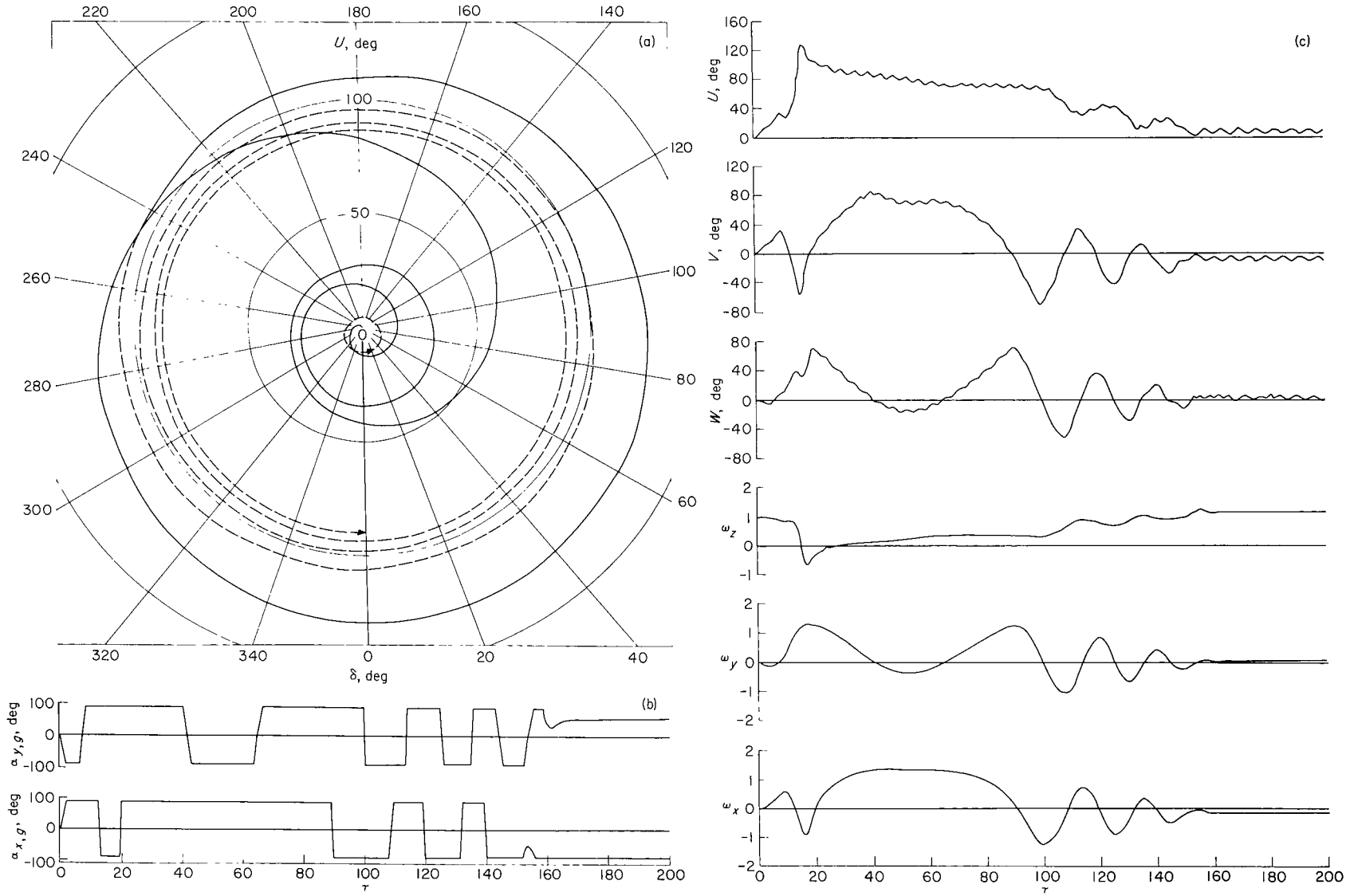

(a) Symmetry-axis trace.

(b) Gimbal angles.

(c) Time history.

Figure 30.- Motion of example station for a general transient product-of-inertia disturbance with a gyroscopic stability system.

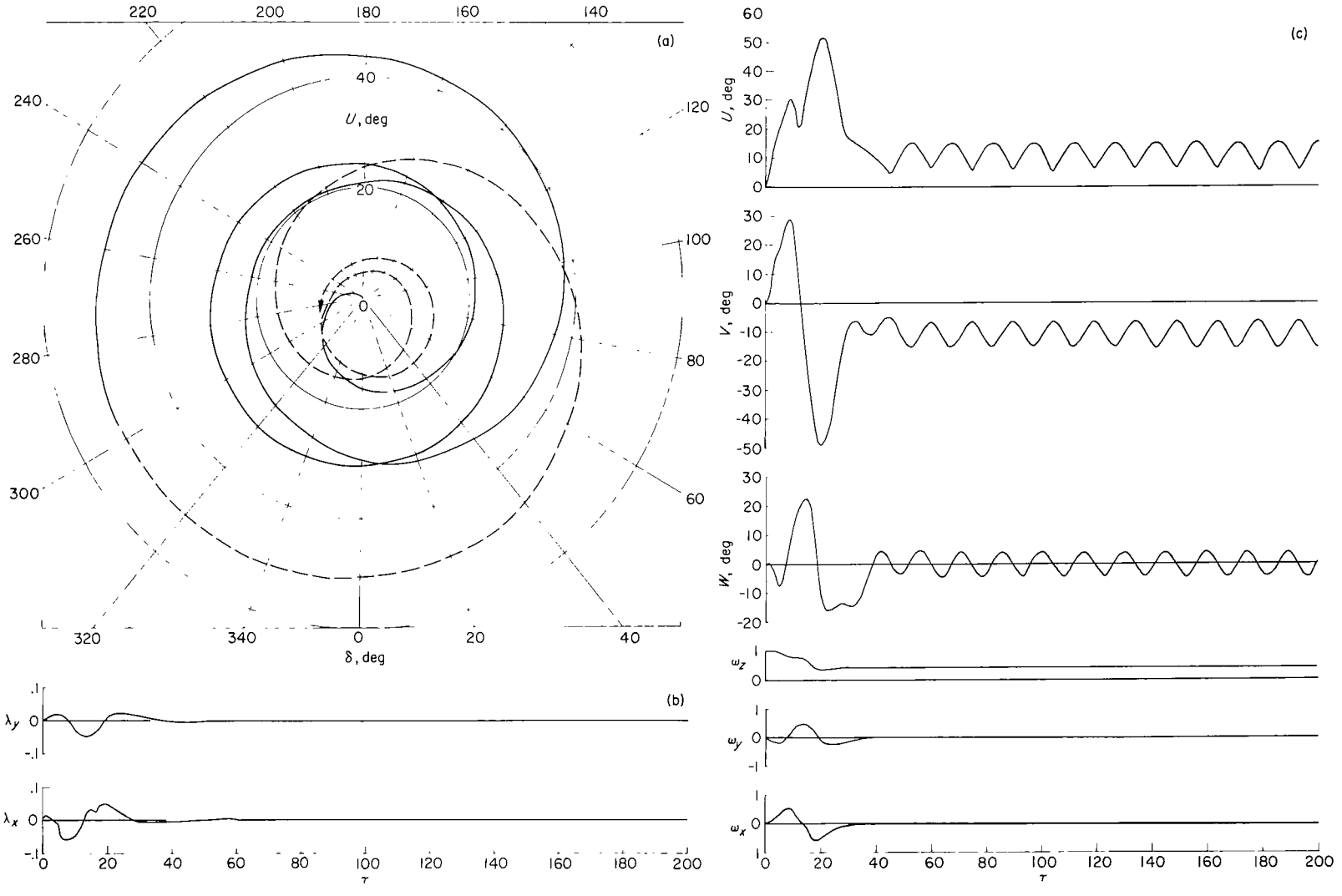

(a) Symmetry-axis trace.

(b) Damping moments.

(c) Time history.

Figure 31.- Motion of example station for a general transient product-of-inertia disturbance with a jet stability system.

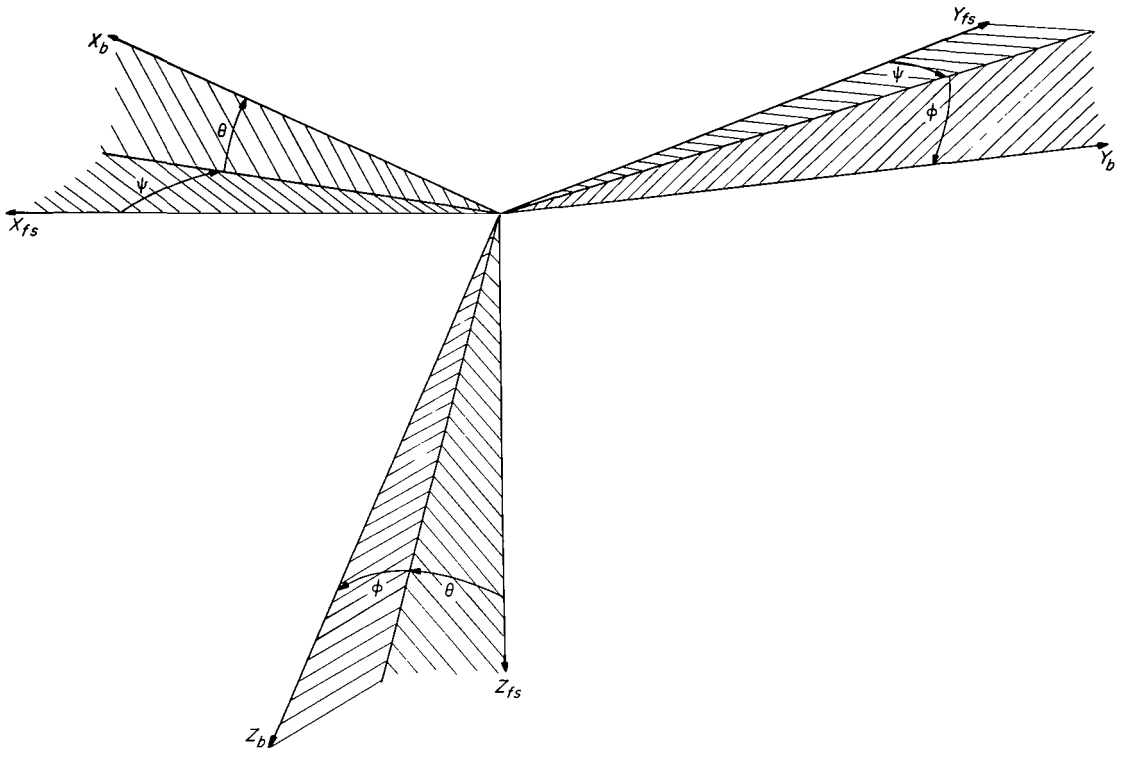

Figure 32.- Orientation of body axes with respect to space-fixed axes by means of Euler angles.

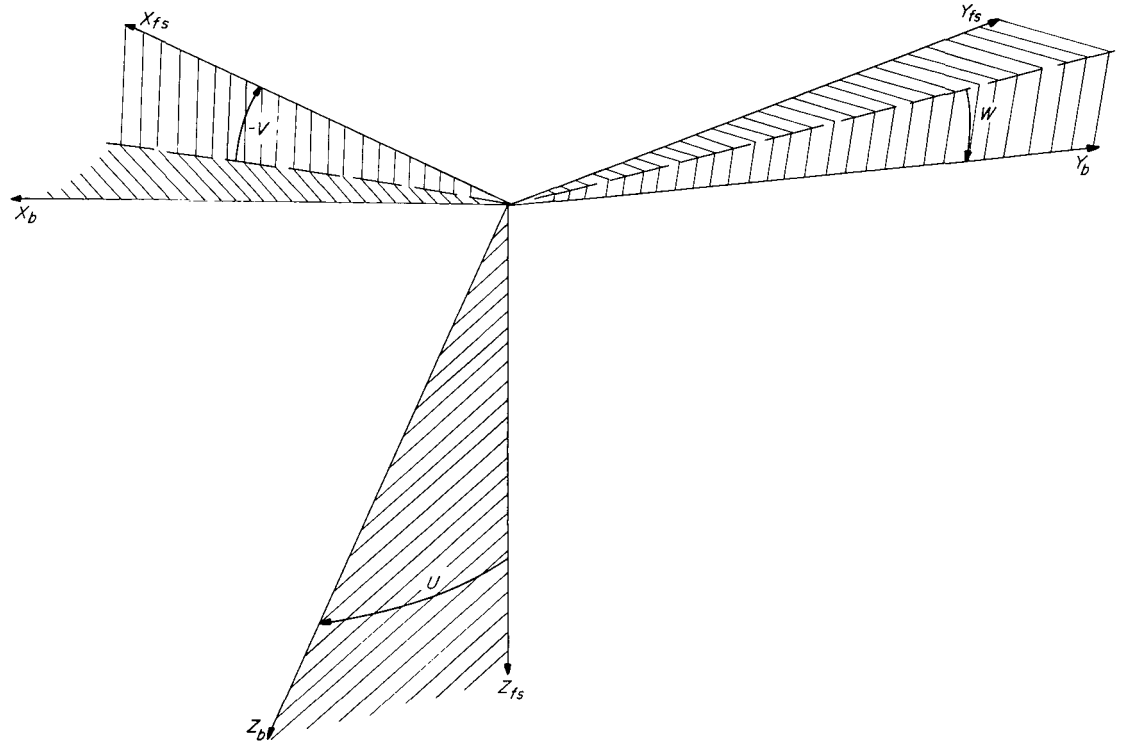

Figure 33.- Orientation of body axes with respect to space-fixed axes by means of stability angles.

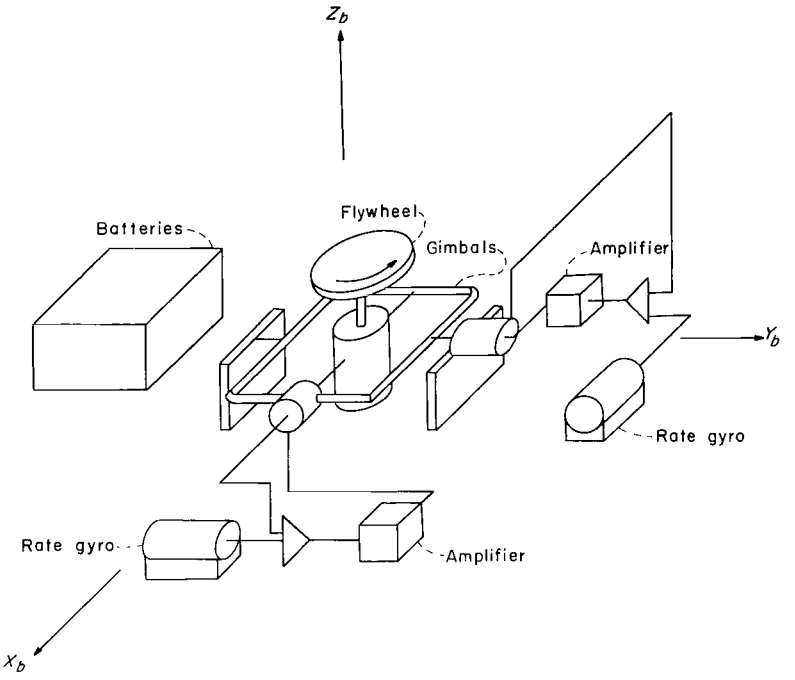

Figure 34.- Schematic of gyroscopic wobble-damper system for space station.

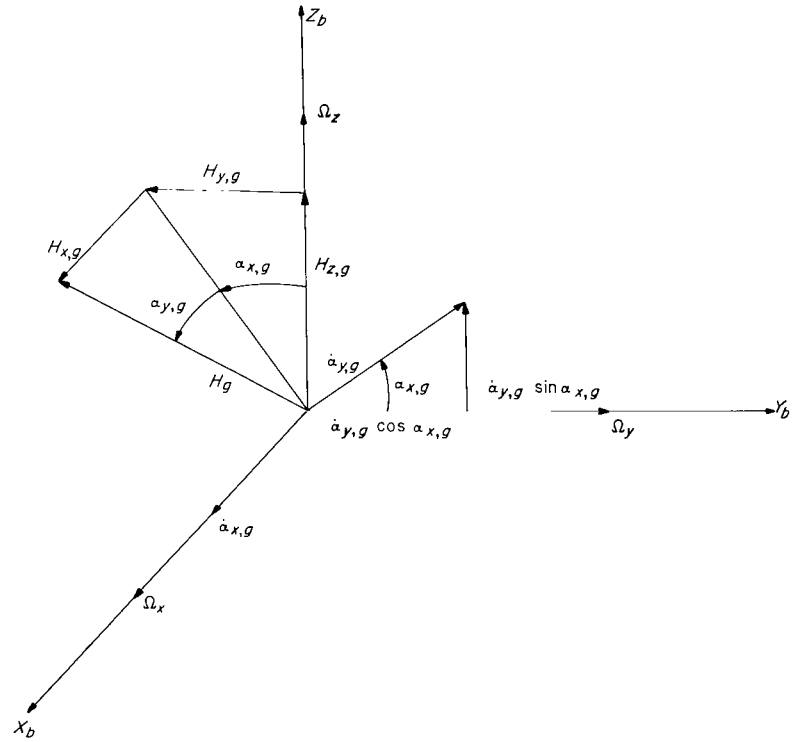

Figure 35.- Orientation of gyroscopic wobble-damper system with respect to space-station axes.

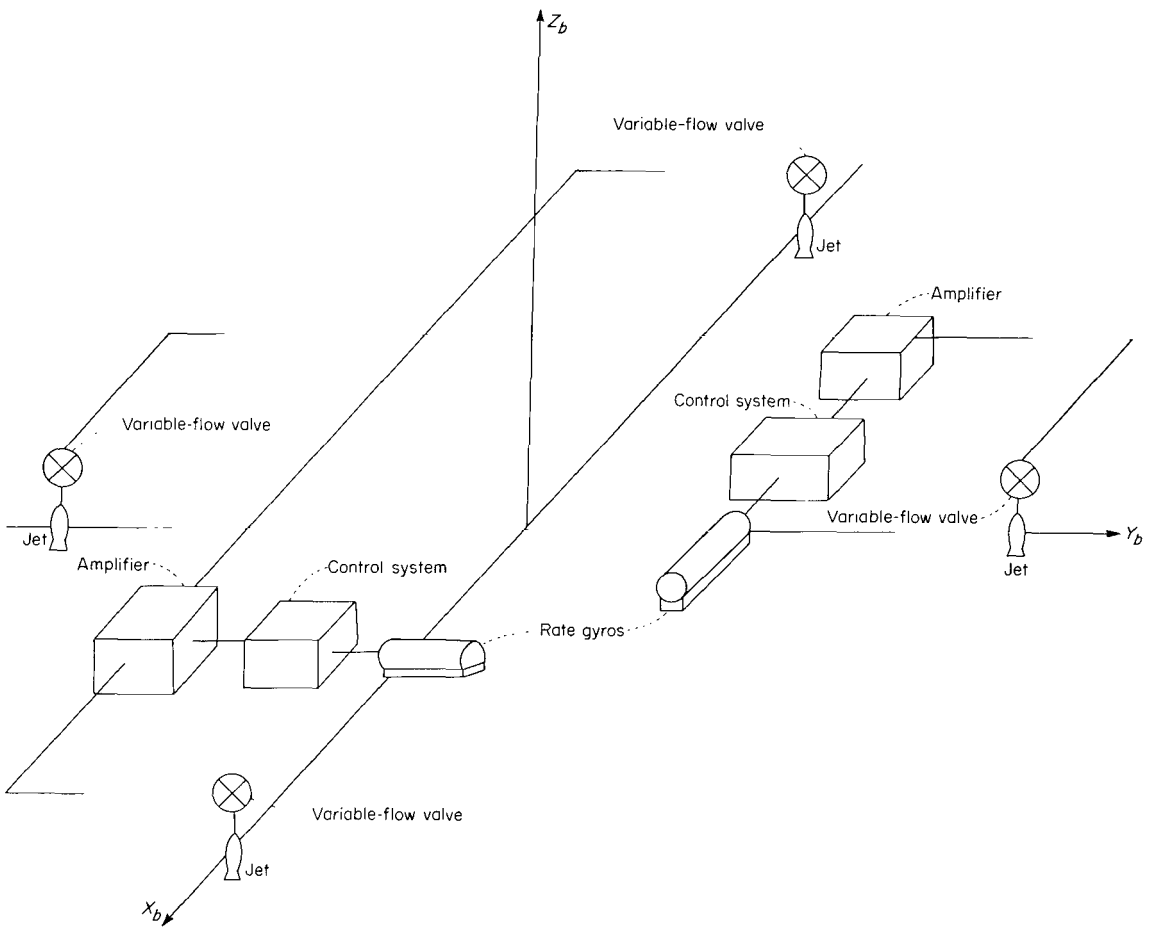

Figure 36.- Schematic of proportional jet damping system for space station.

NASA-Langley, 1964

"The National Aeronautics and Space Administration . . . shall . . . provide for the widest practical appropriate dissemination of information concerning its activities and the results thereof . . . objectives being the expansion of human knowledge of phenomena in the atmosphere and space."

—National Aeronautics and Space Act of 1958

NASA SCIENTIFIC AND TECHNICAL PUBLICATIONS

TECHNICAL REPORTS: Scientific and technical information considered important, complete, and a lasting contribution to existing knowledge.

TECHNICAL NOTES: Information less broad in scope but nevertheless of importance as a contribution to existing knowledge.

TECHNICAL MEMORANDUMS: Information receiving limited distribution because of preliminary data, security classification, or other reasons.

CONTRACTOR REPORTS: Technical information generated in connection with a NASA contract or grant and released under NASA auspices.

TECHNICAL TRANSLATIONS: Information published in a foreign language considered to merit NASA distribution in English.

TECHNICAL REPRINTS: Information derived from NASA activities and initially published in the form of journal articles or meeting papers.

SPECIAL PUBLICATIONS: Information derived from or of value to NASA activities but not necessarily reporting the results of individual NASA-programmed scientific efforts. Publications include conference proceedings, monographs, data compilations, handbooks, sourcebooks, and special bibliographies.

Details on the availability of these publications may be obtained from:

SCIENTIFIC AND TECHNICAL INFORMATION DIVISION

NATIONAL AERONAUTICS AND SPACE ADMINISTRATION

Washington, D.C. 20546